



# Medial preoptic area antagonistically mediates stress-induced anxiety and parental behavior

Guang-Wei Zhang <sup>1</sup>, Li Shen <sup>1</sup>, Can Tao <sup>1</sup>, A-Hyun Jung <sup>1,2</sup>, Bo Peng <sup>1,2</sup>, Zhong Li <sup>1</sup>, Li I. Zhang <sup>1,3</sup>✉ and Huizhong Whit Tao <sup>1,3</sup>✉

**Anxiety is a negative emotional state that is overly displayed in anxiety disorders and depression. Although anxiety is known to be controlled by distributed brain networks, key components for its initiation, maintenance and coordination with behavioral state remain poorly understood. Here, we report that anxiogenic stressors elicit acute and prolonged responses in glutamatergic neurons of the mouse medial preoptic area (mPOA). These neurons encode extremely negative valence and mediate the induction and expression of anxiety-like behaviors. Conversely, mPOA GABA-containing neurons encode positive valence and produce anxiolytic effects. Such opposing roles are mediated by competing local interactions and long-range projections of neurons to the periaqueductal gray. The two neuronal populations antagonistically regulate anxiety-like and parental behaviors: anxiety is reduced, while parenting is enhanced and vice versa. Thus, by evaluating negative and positive valences through distinct but interacting circuits, the mPOA coordinates emotional state and social behavior.**

**A**nxiety is a state of apprehension associated with heightened arousal and vigilance<sup>1–3</sup>. Anxiety after exposure to stress is an adaptive response, as the anxious state helps the animal to maintain caution and cope better with future threats. However, anxiety can become maladaptive in conditions such as post-traumatic stress disorder and major depression, with subjects exhibiting excessive or constant apprehension<sup>2,4,5</sup>. Due to the increasing pressures of life and work in modern society, anxiety disorders are becoming more prevalent and represent a major societal challenge. To improve existing or develop new treatment strategies for anxiety disorders, a thorough understanding of the neural circuits governing this emotional state is necessary.

It was proposed that anxiety is controlled by a large network of distributed brain structures<sup>1,6</sup>. Recent studies were mostly focused on input and output projections of the amygdala and the bed nucleus of the stria terminalis (BNST). Using optogenetic approaches to manipulate neural activity, it was shown that both the amygdala and the BNST play important roles in acutely controlling anxiety-like behaviors<sup>7–9</sup>. In addition, an extra-amygdala circuit, which proceeds from the ventral hippocampus to the lateral septum (LS) and then to the anterior hypothalamus, contributes to the induction and persistence of a stress-induced anxiogenic state by modulating activity in the paraventricular nucleus of the hypothalamus (PVN)<sup>10</sup>. Furthermore, the medial prefrontal cortex interacts with both the ventral hippocampus and the amygdala<sup>11–13</sup> and may modulate anxiety state based on previous experiences or internal needs of the animal<sup>1</sup>. Despite these previous studies, key structures involved in the large anxiety network, especially those critical for the induction and maintenance of anxiety-related phenotypes under different environmental and social contexts, need to be further explored. In addition, circuits through which the anxiety state is coordinated with ongoing behavior remain uncertain.

In the present study, we enacted a strategy to search for brain structures that exhibit both acute and prolonged responses to anxiogenic stressors. Considering a close link between anxiety state

and prior exposure to noxious stimuli<sup>10,14</sup>, brain structures encoding negative valence may be intimately involved in converting emotional valence to the expression of anxiety-like phenotypes. Here, by exploiting acute stress-induced anxiety paradigms, we identified a structure not previously recognized in anxiety-related circuits, the mPOA. It is a sex-dimorphic structure<sup>15,16</sup>, and subsets of its GABAergic neurons were implicated in parental behavior<sup>17–19</sup> and social preference<sup>20</sup>. We found that glutamatergic neurons in the mPOA encode extremely negative valence and mediate anxiety-like behaviors induced by both physical and social stressors. In contrast, GABAergic neurons in the mPOA encode positive valence and produce anxiolytic effects. These two neuronal populations also act opposingly in regulating parental behavior. Our results suggest that by evaluating negative and positive valences with distinct but interacting circuits, the mPOA functions as a critical center for regulating anxiety-like behaviors and antagonistically coordinating the anxiety state and rewarding social behavior.

## Results

**Activation of mPOA glutamatergic neurons by physical stressors.** We subjected mice to several different types of noxious stimuli, such as forced swimming, a heat plate and electric shocks (Fig. 1a and Methods), and tested anxiogenic effects of these stimuli 1 h later by using two standard behavioral assays: the open-field test (OFT) and the elevated plus maze (EPM) test<sup>7,8,10,21</sup>. In the OFT (Fig. 1b), mice exposed to either one of the stressors spent less time in the center zone than did the respective control animals experiencing the same experimental contexts in a 20-min test session (Fig. 1c, see control conditions in Extended Data Fig. 1a,b). In the EPM test (Fig. 1d), the open-arm time in a 5-min test session for mice exposed to stressors was reduced compared with that of control animals (Fig. 1e). These behavioral results suggest an elevated anxiety state after exposure to stressors, consistent with previous studies<sup>7,14,21,22</sup>.

Next, we examined which brain areas exhibited acute or prolonged activity after stress exposure by c-Fos staining (Extended

<sup>1</sup>Zilkha Neurogenetic Institute, University of Southern California, Los Angeles, CA, USA. <sup>2</sup>Graduate Program in Neuroscience, University of Southern California, Los Angeles, CA, USA. <sup>3</sup>Department of Physiology and Neuroscience, Keck School of Medicine, University of Southern California, Los Angeles, CA, USA. ✉e-mail: [liizhang@usc.edu](mailto:liizhang@usc.edu); [htao@usc.edu](mailto:htao@usc.edu)

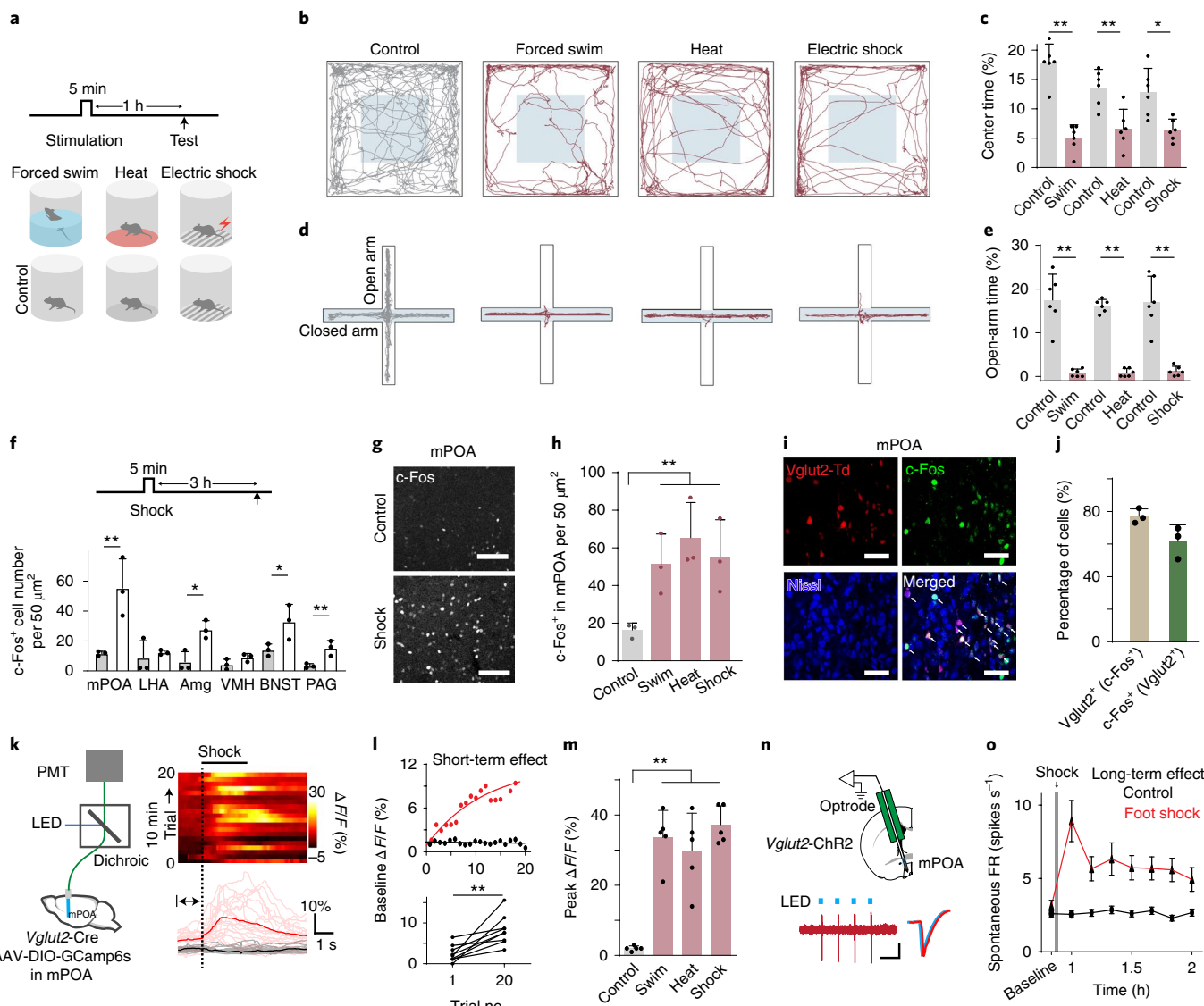


**Fig. 1 | mPOA glutamatergic neurons are activated by physical stress.** **a**, Experimental timeline for measuring anxiety-like behaviors following a 5-min treatment with either forced swimming, a heat plate or electric shocks of 0.5 Hz and 0.3 mA. **b**, Tracing of locomotion for representative control (gray) and experimental (dark red) animals exposed to different stressors. Light gray squares mark the designated center zone. **c**, Quantification of percent time spent in the center zone during the OFT ( $n=6$  animals for each group, three males and three females;  $*P < 0.05$ ,  $**P < 0.01$ , two-way ANOVA and post hoc test). **d**, Locomotion traces for representative control and stressor-exposed animals. Closed arms are indicated with light gray. **e**, Quantification of percent time spent in the open arms of the EPM ( $n=6$  animals for each group, three males and three females;  $**P < 0.01$ , two-way ANOVA and post hoc test). **f**, Quantification of the number of c-Fos<sup>+</sup> cells per 50  $\mu\text{m}^2$  in different brain regions. Amg, amygdala; VMH, ventromedial hypothalamus.  $*P < 0.05$ ,  $**P < 0.01$ , two-way ANOVA and post hoc test,  $n=3$  animals. Top inset: experimental timeline for c-Fos staining. **g**, Representative confocal images of c-Fos staining in the mPOA for a control and an experimental animal exposed to electric shocks. Scale bar, 50  $\mu\text{m}$ . **h**, Quantification of the number of c-Fos<sup>+</sup> neurons in the mPOA for each treatment ( $n=3$  animals for each group;  $**P < 0.05$ , one-way ANOVA and post hoc test; data from control animals were combined). **i**, Representative images showing colocalization of Vglut2 (reflected by tdTomato expression in Vglut2-Cre-Ai14 mice) and c-Fos (green) signals. Blue represents Nissl staining. Scale bar, 25  $\mu\text{m}$ . **j**, Quantification of the percentage of Vglut2<sup>+</sup> cells in the c-Fos<sup>+</sup> population (brown) and of the percentage of c-Fos<sup>+</sup> cells in the Vglut2<sup>+</sup> population (green). **k**, Left: experimental setup for photometry. PMT, photomultiplier tubes. Right: heatmap of calcium signals in an example animal for 20 trials of electric shocks (duration marked by a thick dark line). Bottom: averaged traces for the shock (solid red) and control (solid black, with no current output) conditions, with pale colors indicating individual trials. The dotted line marks the onset of shocks. **l**, Top: baseline fluorescence signals within a 1-s window in the same animal shown in **k** just before shock-onset over 20 trials (red). Black denotes a control animal.  $P < 0.001$ , Kolmogorov-Smirnov test with Bonferroni correction. Bottom: baseline fluorescence signal at the first and 20th trials for nine animals.  $**P < 0.01$ , two-sided paired t-test. **m**, Quantification of stressor-induced peak  $\Delta F/F$  (%) for control and exposed animals ( $n=5$  for each group, three males and two females;  $**P < 0.01$ , one-way ANOVA and post hoc test; data from control animals were combined). **n**, Top: diagram for optrode recording from the mPOA in head-fixed Vglut2-Cre-ChR2 mice. Bottom: sample recorded traces of spiking of a ChR2-expressing mPOA glutamatergic neuron in response to pulses of LED stimulation (blue dots). Right inset: comparison of spike waveforms (slightly offset) spontaneously generated (red) or evoked by LED stimulation (blue) of the same unit. **o**, Spontaneous firing rates (FRs) across time (bin size: 10 min) before and after exposure to electric shocks (marked by the vertical gray bar).  $P < 0.001$ , two-sided Kolmogorov-Smirnov test with Bonferroni correction;  $n=35$  and  $n=29$  neurons for control and experimental groups, respectively. Error bars represent s.e.m. Images in **g** are representative of  $n=3$  animals. Data in **i** are representative of  $n=3$  animals. (Extended Data Fig. 1; see Supplementary Data for detailed statistics).

Data Fig. 1c,d and Methods). Animals were killed 3 h after stress exposure, as it takes about 2–3 h for c-Fos protein expression to peak after neuronal activation<sup>23</sup>. A higher level of c-Fos expression was observed in the mPOA of animals exposed to electric shocks than that in control animals (Fig. 1f,g). Increased staining was also observed in the amygdala, BNST and periaqueductal gray (PAG) (Fig. 1f), the three structures that were previously implicated in anxiety<sup>1,3</sup>. Similarly, increased c-Fos expression was observed in the mPOA after exposure to other types of stressors (Fig. 1h). About 80% of activated mPOA neurons were glutamatergic, as shown by the colocalization of c-Fos and vesicular-glutamate transporter (Vglut)2 signals (Fig. 1i,j), and about 60% of glutamatergic neurons in the mPOA were activated after exposure to electric shocks (Fig. 1j). Neurons activated by different stressors appeared to be randomly distributed in the mPOA (Extended Data Fig. 1e), considering the endogenous expression pattern of Vglut2 (Extended Data Fig. 1f,g).

We next directly examined whether glutamatergic neurons in the mPOA could be acutely activated by physical stressors. By injecting an adeno-associated virus (AAV) encoding Cre-dependent GCaMP6s into the mPOA of *Slc17a6-Cre* (*Vglut2-Cre*) mice<sup>24</sup>, we monitored calcium signals in freely moving animals with photometry<sup>25</sup> (Fig. 1k). All testing stressors induced large increases of calcium signals (Fig. 1k,m and Extended Data Fig. 2a–d), confirming that mPOA glutamatergic neurons can be acutely activated by various types of stressors. Control experiments showed no or minimal motion artifacts under our experimental conditions (Extended Data Fig. 2e–k). In addition, we noticed that the baseline fluorescence preceding the onset of shocks gradually increased with repeated applications (Fig. 1l and Extended Data Fig. 3a), suggesting that the spontaneous firing activity might be increased. As photometry data lacked single-cell resolution, to further examine the spontaneous activity of mPOA glutamatergic neurons, we recorded signals from optogenetically identified glutamatergic neurons (onset latency of light-evoked spikes,  $2.8 \pm 0.8$  ms, mean  $\pm$  s.d.) using optrodes in *Vglut2*-channelrhodopsin (Chr2) mice (Fig. 1n and Extended Data Fig. 3b). Indeed, the spontaneous firing rate of these neurons was increased for hours after the cessation of electric shocks but remained stably low in control animals (Fig. 1o and Extended Data Fig. 3c). Overall, the increase persisted for about 4 h (Extended Data Fig. 3d), consistent with the behavioral result of an elevated anxiety state for about 4 h after stress exposure (Extended Data Fig. 3e). Furthermore, nearly all recorded mPOA glutamatergic neurons responded acutely to multiple types of stressors (Extended Data Fig. 3f,g). Of non-phototagged neurons (presumably GABAergic neurons), 54% showed no acute response to stress, 23% were activated, and 23% were suppressed (Extended Data Fig. 3h). The spontaneous firing rate of these neurons was essentially unchanged after stress exposure (Extended Data Fig. 3i). Together, our results suggest that mPOA glutamatergic neurons respond acutely to a variety of stressor stimuli and their baseline activity increases for a considerably long period of time after exposure to stress.

**Activation of glutamatergic mPOA neurons induces negative valence and anxiety-like behaviors.** To test whether the mPOA is involved in stress-induced anxiety, we optogenetically stimulated mPOA glutamatergic neurons by virally expressing Chr2 in *Vglut2-Cre* mice (Fig. 2a and Extended Data Fig. 4a,b). We first confirmed the high efficacy of Chr2 activation using slice whole-cell recordings (Fig. 2b). By injecting currents (square or ramp) into the recorded cells, we found that mPOA glutamatergic neurons could be driven to fire action potentials at frequencies up to  $\sim 15$  Hz (Fig. 2c). Because these neurons could be activated by aversive stimuli, we tested whether their activity encoded negative valence by using a two-chamber real-time place preference test (PPT)<sup>8,26,27</sup>. Light-emitting diode (LED) stimulation was applied whenever the

animal stayed in the designated stimulation (LED-on) chamber (Fig. 2d). Chr2-expressing animals spent much less time in the LED-on chamber than did GFP control animals, with the latter spending approximately equal amounts of time in randomly assigned LED-on and LED-off chambers (Fig. 2e and Supplementary Videos 1 and 2). No obvious sex difference was observed (Fig. 2e). Thus, activation of mPOA glutamatergic neurons is aversive. In addition, 24 h after exposure to LED stimulation, animals still exhibited avoidance from the LED-on chamber, even though no LED light was applied (Extended Data Fig. 5a,b), indicating that activation of mPOA neurons can drive conditioned place avoidance.

We further examined whether increasing mPOA glutamatergic neuron activity could acutely enhance anxiety-like behaviors (Fig. 2f). Compared with GFP control animals, activation with continuous LED light pulses (at 10 Hz) reduced the center time in the OFT (Fig. 2g) and the open-arm time in the EPM test (Fig. 2f,h), and similar effects were observed for both sexes. These effects increased with increasing stimulation frequencies (Extended Data Fig. 5c,d). Meanwhile, optogenetic stimulation induced pupil dilation (Fig. 2i,j) and increased locomotion (Fig. 2k) without any location specificity (Extended Data Fig. 5e–h). These behavioral patterns are suggestive of high arousal levels<sup>28</sup>, consistent with the notion that anxiety is associated with elevated arousal and vigilance<sup>1–3</sup>.

We also applied chemogenetics for activating mPOA glutamatergic neurons, by expressing a Cre-dependent excitatory designer receptor exclusively activated by designer drugs (DREADD) receptor, human (h)M3Dq (Extended Data Fig. 4c). In slice recordings, we confirmed that application of the DREADD agonist clozapine-N-oxide (CNO) induced depolarization of membrane potential (and increased firing rate) in hM3Dq-expressing mPOA neurons (Extended Data Fig. 5i–k). In freely moving animals, chemogenetic activation by CNO administration reduced the center time in the OFT and open-arm time in the EPM test as compared with mCherry control animals (Extended Data Fig. 5l,m). In addition, optogenetic stimulation of mPOA glutamatergic neurons for 5 min resulted in elevated anxiety-like behaviors 1 h after stimulation (Extended Data Fig. 5n–p), suggesting that the activity of these neurons promotes the initiation of an anxiety state.

Strong activation of mPOA glutamatergic neurons (at 15 Hz) apparently caused extremely aversive emotion. In conflict tests in which a physical stressor (electric shocks, a heat plate or cold water) was present in the LED-off side of a test box, Chr2-expressing animals avoided the LED-on side (Extended Data Fig. 6a–c and Supplementary Videos 3 and 4). In addition, in a single-chamber box, the strong activation of mPOA glutamatergic neurons greatly increased the frequency of rearing and even more dramatically triggered animal jumping (Extended Data Fig. 6d–g). It also suppressed food intake in hungry mice (Extended Data Fig. 6h). Similar effects were observed in animals with chemogenetically activated mPOA glutamatergic neurons (Extended Data Fig. 6i–k). These behavioral results suggest that mPOA glutamatergic neurons can encode strongly negative valence.

**Suppression of mPOA glutamatergic neurons reduces anxiety-like behaviors.** To further test whether mPOA glutamatergic neurons mediate stress-induced anxiety, we silenced these neurons by expressing a Cre-dependent inhibitory DREADD receptor, hM4Di (Extended Data Fig. 4d). Slice whole-cell recording confirmed that application of CNO could prevent spiking of hM4Di-expressing mPOA neurons (Fig. 3a,b). In the OFT, hM4Di-expressing animals injected with CNO at 40 min after stress exposure spent more time in the center zone than did mCherry control animals and saline-injected hM4Di-expressing animals (Fig. 3c,d). Similarly, the open-arm time in the EPM test also largely increased in CNO-injected hM4Di-expressing animals (Fig. 3e,f). These results indicate that silencing mPOA glutamatergic neurons suppresses stressor-induced anxiety-like behaviors.

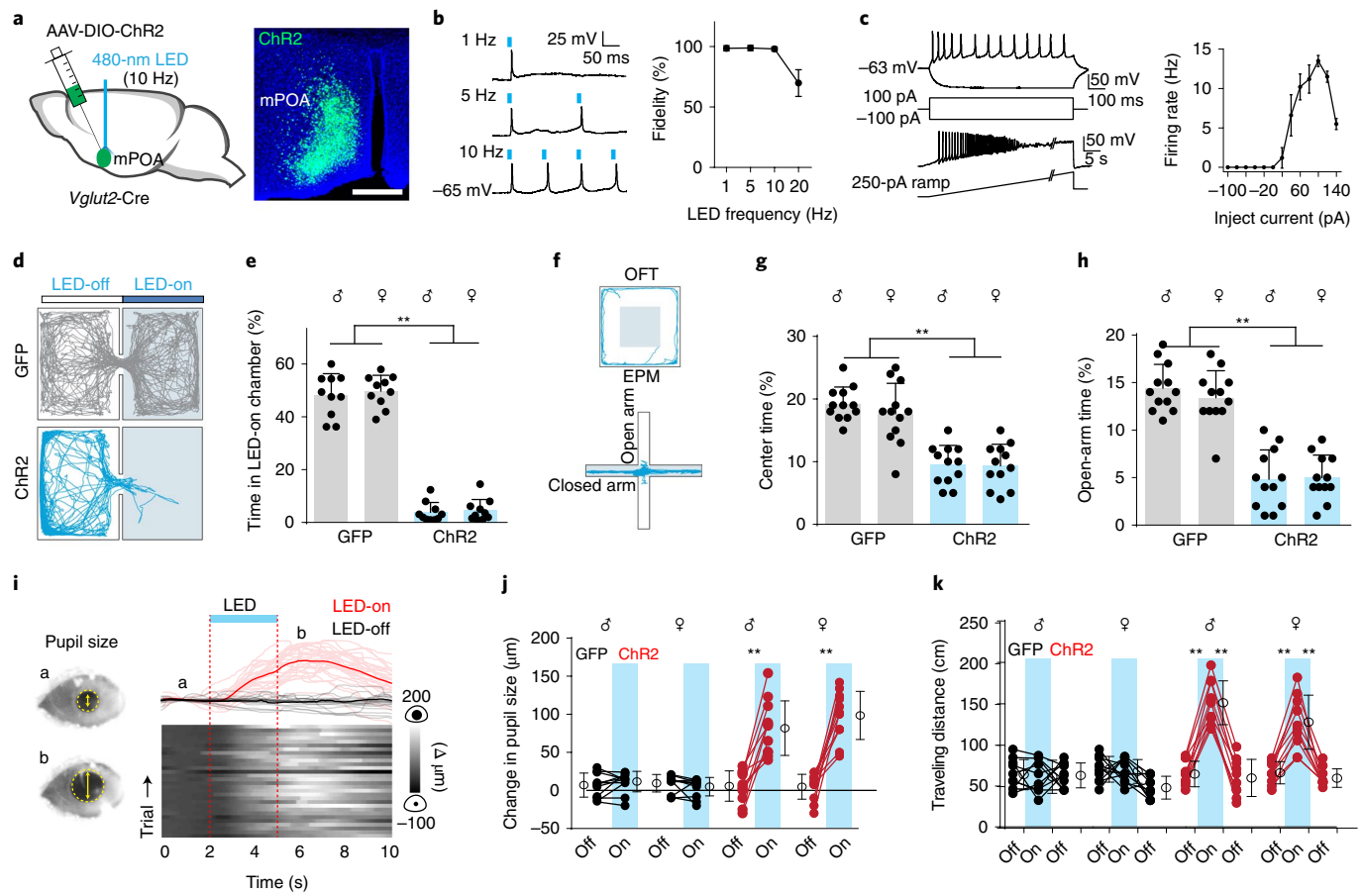


**Fig. 2 | Activating mPOA glutamatergic neurons enhances anxiety-like behaviors.** **a**, Left: injection and stimulation configuration. Right: representative image showing the expression of ChR2-enhanced (e)YFP in the mPOA. Scale bar, 500 μm. **b**, Left: example traces of spiking of a recorded mPOA glutamatergic neuron in response to pulses of blue light at 1, 5 and 10 Hz. Right: fidelity of spiking at different stimulation frequencies ( $n=10$  cells). Error bars represent s.e.m. **c**, Left: example membrane potential responses to injections of square (top) or ramp (bottom) current. The resting membrane potential was  $-63\text{ mV}$ . Right: average firing rates in response to injected currents at different amplitudes ( $n=10$  cells). Error bars represent s.e.m. **d**, Representative locomotion tracing for a GFP control and a ChR2-expressing animal in the two-chamber PPT. **e**, Quantification of percent time in the LED-on chamber.  $**P < 0.01$ , two-sided Mann-Whitney test with Bonferroni correction,  $n=10$  animals for each group. Males and females are displayed separately. Error bars represent s.d. **f**, Locomotion tracing for an example ChR2-expressing animal with continuous photostimulation in the OFT (top) or the EPM (bottom). **g**, Quantification of center time in the OFT.  $**P < 0.01$ , two-sided Mann-Whitney test with Bonferroni correction,  $n=12$  animals for each group. Error bars represent s.d. **h**, Quantification of open-arm time in the EPM test.  $**P < 0.01$ , two-sided Mann-Whitney test with Bonferroni correction,  $n=12$  for each group. Error bars represent s.d. **i**, Changes in pupil size in 60 trials of photostimulation (LED-on and LED-off trials were randomly assigned). Top: average change in pupil size in the LED-on (solid red) and LED-off (solid black) conditions. Pale colors represent individual trials. Bottom: heatmap for change in pupil size in different trials aligned by the onset of LED stimulation (blue bar). Left inset: sample images of the eye at time points a and b. **j**, Average changes in pupil size in LED-off and LED-on conditions.  $**P < 0.01$ , two-sided paired t-test,  $n=11$  animals for each group. Data points for the same animal are connected with a line. Error bars represent s.d. **k**, Traveling distance in an open arena in LED-off (3 min per block) and LED-on (3 min) conditions.  $**P < 0.01$ , two-way repeated-measures ANOVA,  $n=10$  animals for each group. Error bars represent s.d. Images in **a** are representative of  $n=3$  animals. (see Supplementary Data for detailed statistics).

In a parallel set of experiments, we optogenetically silenced mPOA glutamatergic neurons by expressing Cre-dependent archaerhodopsin (ArchT) (Extended Data Fig. 4e). Slice whole-cell recording confirmed that green LED light induced a membrane hyperpolarization in ArchT-expressing mPOA neurons that prevented their spiking (Fig. 3g,h). Optogenetic silencing of mPOA glutamatergic neurons resulted in a weak place preference (Extended Data Fig. 6l–n). We next tested optogenetic silencing in the OFT 1 h after exposure to electric shocks (Fig. 3i), with LED-off and LED-on blocks (3 min per block) interleaved during the test. In LED-on blocks, the ArchT-expressing animals exhibited significantly more center time than did GFP control animals, whereas in LED-off blocks, these two groups of animals did not

show a significant difference (Fig. 3j). In the EPM test, optogenetically silenced animals had an increased open-arm time compared with GFP control animals (Fig. 3k,l).

Together, the results of the above activation and inactivation experiments suggest that mPOA glutamatergic neurons mediate the expression of physical stress-induced anxiety-like behaviors. We further tested the role of these neurons in the induction of anxiety-like behaviors by optogenetically silencing them only during exposure to shocks. This resulted in increases in center time and open-arm time compared with GFP control animals (Extended Data Fig. 6o,p), indicating that acute responses of mPOA glutamatergic neurons to stressors may be required for the induction of anxiety-like behaviors.

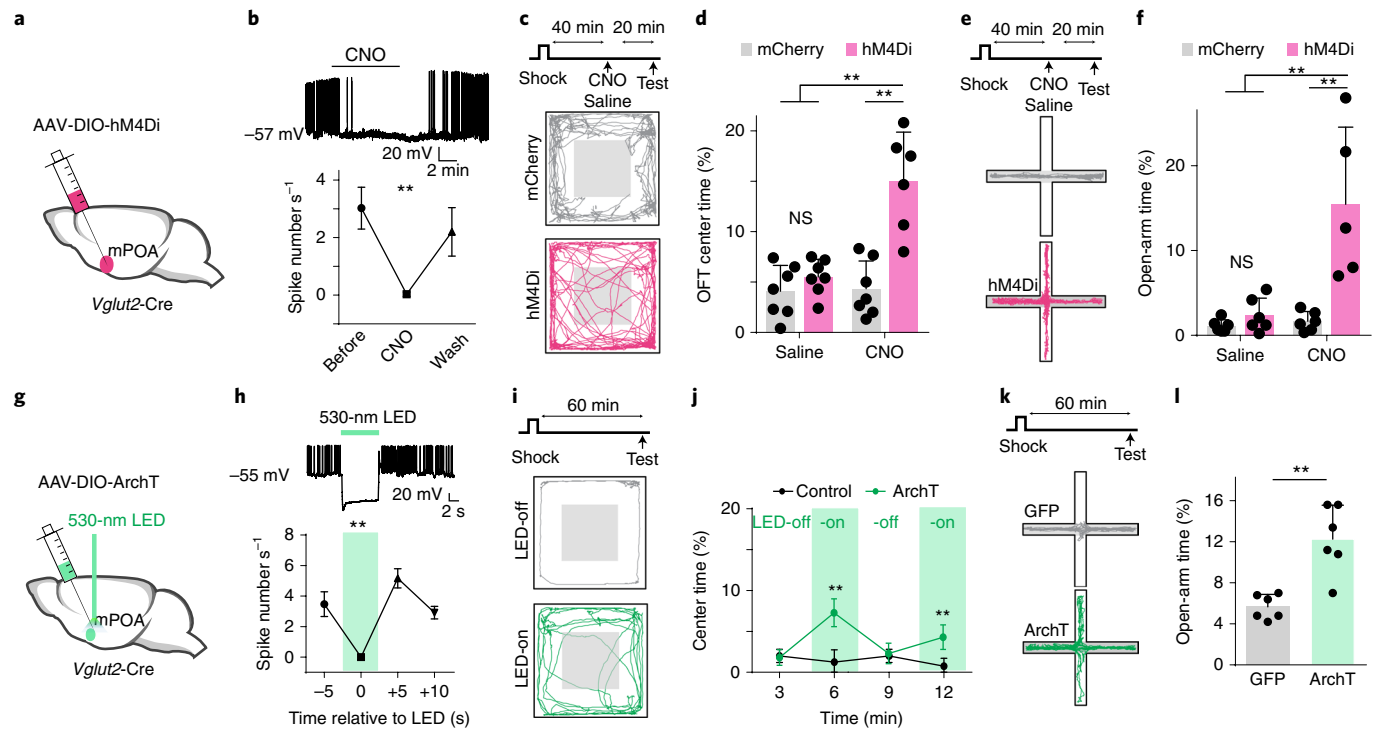


**Fig. 3 | Silencing mPOA glutamatergic neurons reduces stress-induced anxiety-like behaviors.** **a**, Viral injection for chemogenetic silencing. **b**, Top: raw trace of current-clamp recording from an hM4Di-expressing mPOA glutamatergic neuron in the slice preparation. Bottom: average spontaneous spike frequencies before and after perfusion with CNO, as well as after washing out CNO. \*\* $P < 0.01$ , one-way repeated-measures ANOVA,  $n = 5$  cells from two mice. Error bars represent s.d. **c**, Movement tracing for an example mCherry control (gray) and an hM4Di-expressing (red) animal in the OFT 1 h after exposure to electric shocks, injected with CNO at 40 min. Top inset: experimental timeline. **d**, Percentage of center time in the OFT for mCherry control and hM4Di-expressing animals after shock exposure. \*\* $P < 0.01$ , two-sided Mann–Whitney test,  $n = 7$  and  $n = 6$  mice, respectively (three males). Saline control experiments were performed on a different day for the same animal. Error bars represent s.d. **e**, Movement tracing for an mCherry control (gray) and an hM4Di-expressing (red) animal in the EPM test after exposure to electric shocks. **f**, Percentage of open-arm time in the EPM test for mCherry control and hM4Di-expressing animals after shock exposure. \*\* $P < 0.01$ , two-sided Mann–Whitney test,  $n = 6$  and  $n = 5$  mice, respectively (three males). Error bars represent s.d. **g**, Viral injection and stimulation for optogenetic silencing. **h**, Top: membrane potential response to green LED stimulation in an ArchT-expressing mPOA glutamatergic neuron in the slice preparation. Bottom: average spontaneous spike rates before, during and after LED stimulation (marked by the green rectangle). \*\* $P < 0.01$ , one-way repeated-measures ANOVA,  $n = 5$  cells from two mice. Error bars represent s.e.m. **i**, Movement tracing for an ArchT-expressing animal in the OFT in an LED-off (gray) and an LED-on (green) block. **j**, Percentage of center time for GFP control (black) and ArchT-expressing (green) animals in LED-off and LED-on blocks in the OPT. \*\* $P < 0.01$ , two-way repeated-measures ANOVA,  $n = 8$  and  $n = 9$  animals (four males) for control and ArchT groups, respectively. Error bars represent s.e.m. **k**, Movement tracing for a GFP control (gray) and an ArchT-expressing animal (green) in the EPM test. **l**, Percentage of open-arm time for GFP control and ArchT-expressing animals. \*\* $P < 0.01$ , two-sided Mann–Whitney test,  $n = 6$  animals (three males) for each group. Error bars represent s.d. (see Supplementary Data for detailed statistics).

**mPOA antagonistically regulates social stress-induced anxiety and parental behavior.** Previously, the mPOA was implicated in social behaviors, such as parenting and social preference<sup>18–20</sup>. We wondered whether this structure could also play a role in socially induced anxiety. Following the method in a previous study<sup>19</sup>, we introduced a younger male mouse (intruder) or a foreign pup into the home cage of a resident virgin male for 15 min. This resulted in elevated anxiety-like behaviors in the resident, as shown by the OFT and the EPM test performed at 40 min after the exposure (Extended Data Fig. 7a,b). Thus, male intruders and foreign pups are social stressors to virgin males. Using fiber photometry, we imaged the calcium activity of mPOA glutamatergic neurons during social interactions (Fig. 4a). We found that, in virgin male mice, bouts of interaction with an intruder or a pup elicited large increases in calcium activity in mPOA glutamatergic neurons (Fig. 4b–d). By contrast, no increase in calcium activity was observed when a virgin male interacted with a female intruder or when a virgin female interacted with a foreign pup (Fig. 4e,f). These results indicate that mPOA glutamatergic neurons can be activated by social stressors but not by social rewards.

Optogenetically silencing mPOA glutamatergic neurons during the OFT and the EPM test, performed after exposure to social stress, reduced anxiety-like behaviors (Fig. 4g,h), suggesting that these neurons also mediate the expression of social stress-induced anxiety-like behaviors. Silencing these neurons during the 15-min exposure to a male intruder greatly reduced chances of the resident male fighting the intruder (Fig. 4i), indicating reduced intermale aggression<sup>19</sup>, which is possibly attributed to reduced anxiety<sup>20</sup>. In addition, the treatment impaired the expression of anxiety-like behaviors after intruder exposure (Fig. 4j), suggesting that activity of mPOA glutamatergic neurons is also required for the induction of social anxiety.

We also tested anxiety-like behaviors induced by pup exposure. Optogenetic silencing of mPOA glutamatergic neurons after exposure reduced anxiety-like behaviors (Fig. 4k,l). During pup exposure, the virgin male displayed pup-directed aggression (Fig. 4m) as reported previously<sup>19</sup>. Photoactivation of mPOA glutamatergic neurons whenever the male started to explore the pup largely suppressed pup attack (Fig. 4m) and increased the duration of pup grooming (Extended Data Fig. 7c), indicating reduced pup-directed

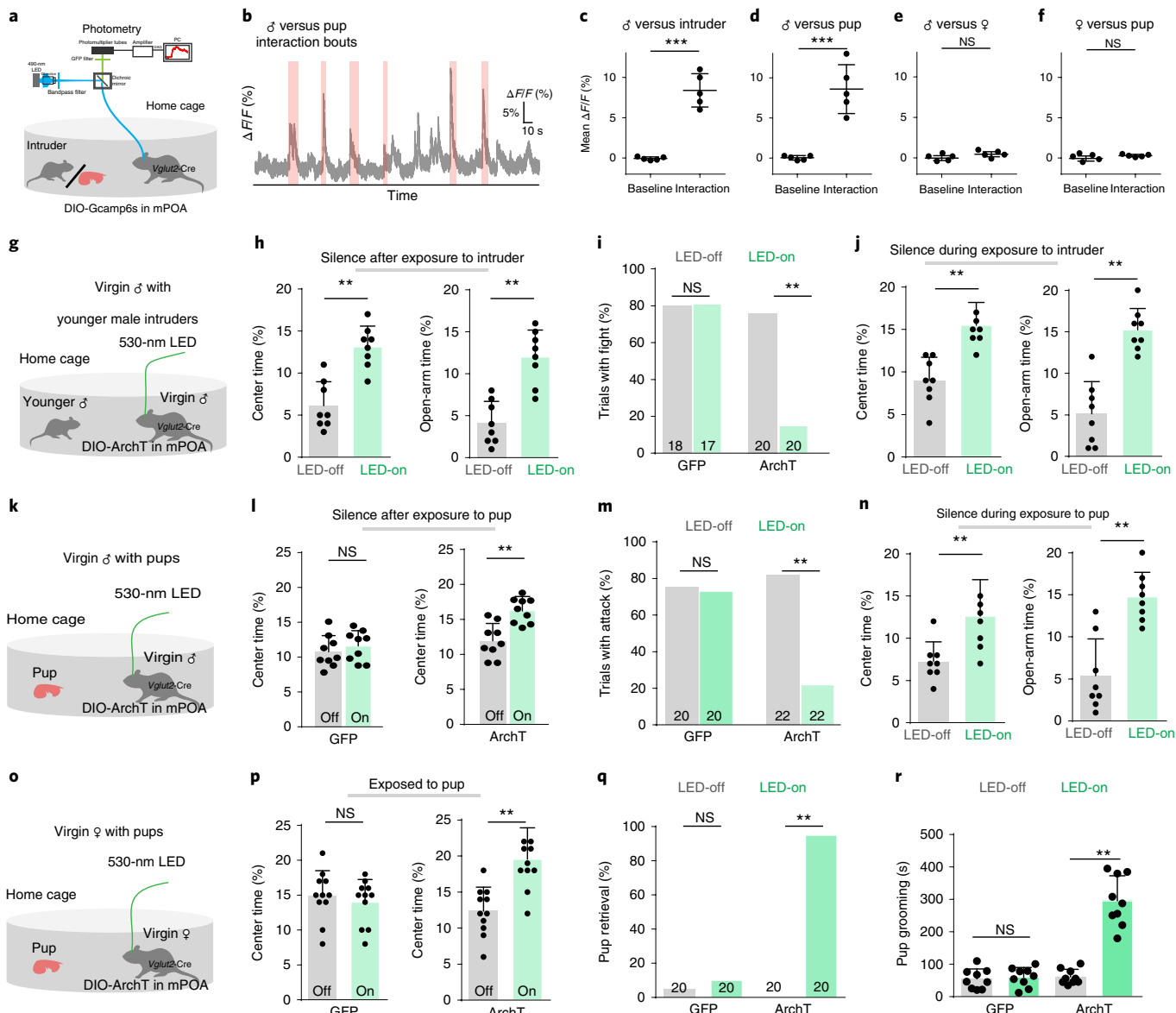


**Fig. 4 | mPOA glutamatergic neurons antagonistically regulate social stress-induced anxiety and parental behavior.** **a**, Exposing a resident mouse to a pup or a younger intruder while imaging ensemble calcium activity of mPOA glutamatergic neurons using photometry. DAQ, data acquisition board; PC, personal computer. **b**, A representative trace for GCaMP6s fluorescence change in a virgin male when exposed to a pup. Colored bars indicate bouts of interaction with the pup. **c-e**, Percentage changes in fluorescence in virgin males before and after placing a male intruder (**c**), a pup (**d**) or a female (**e**) in the home cage. \*\*\* $P < 0.01$ , two-sided Mann-Whitney test,  $n = 5$  animals. Error bars represent s.d. **f**, Percentage changes in fluorescence in virgin females ( $n = 5$ ) before and after placing a pup in the cage. Error bars represent s.d. **g**, Experimental condition: a virgin male exposed to a younger male intruder. **h**, Percentage of center time in the OFT (left) and of open-arm time in the EPM test (right) for intruder-exposed resident males in LED-off (gray) and LED-on (green) conditions. \*\* $P < 0.01$ , two-sided Mann-Whitney test,  $n = 8$  ArchT-expressing animals. Error bars represent s.d. **i**, Percentage of trials in which the resident fought the intruder in LED-off (gray) and LED-on (green) conditions for GFP control and ArchT-expressing animals. \*\* $P < 0.01$ , two-sided Fisher's exact test with Bonferroni correction,  $n = 8$  animals in each group; NS, not significant. Total numbers of trials are marked. **j**, Percentage of center times in the OFT (left) and of open-arm times in the EPM test (right) without (gray) and with (green) optogenetic silencing of mPOA glutamatergic neurons during exposure to the intruder. \*\* $P < 0.01$ , two-sided Mann-Whitney test,  $n = 8$  ArchT-expressing animals. Error bars represent s.d. **k**, Experimental condition: a virgin male exposed to a pup. **l**, Percentage of center times in the OFT for GFP control (left,  $n = 9$ ) and ArchT-expressing (right,  $n = 9$ ) animals in LED-off (gray) and LED-on (green) conditions. \*\* $P < 0.01$ , Mann-Whitney test. Error bars represent s.d. **m**, Percentage of trials with the virgin male attacking the pup in LED-off and LED-on conditions for GFP control ( $n = 9$ ) and ArchT-expressing ( $n = 9$ ) animals. \*\* $P < 0.01$ , Fisher's exact test with Bonferroni correction. Total numbers of trials are marked. **n**, Percentage of center times in the OFT (left) and of open-arm times in the EPM test (right) for pup-exposed males without (gray) and with (green) optogenetic silencing of mPOA glutamatergic neurons during pup exposure. \*\* $P < 0.01$ , Mann-Whitney test,  $n = 8$  ArchT-expressing animals. Error bars represent s.d. **o**, Experimental condition: a resident virgin female exposed to a pup. **p**, Percentage of center times in the OFT for GFP control (left,  $n = 11$ ) and ArchT-expressing (right,  $n = 11$ ) animals in LED-off (gray) and LED-on (green) conditions. \* $P < 0.05$ , Mann-Whitney test with Bonferroni correction. Error bars represent s.d. **q**, Percentage of trials with pup retrieval for GFP control ( $n = 11$ ) and ArchT-expressing ( $n = 11$ ) female mice in LED-off and LED-on conditions. \*\* $P < 0.01$ , Fisher's exact test with Bonferroni correction. **r**, Total duration of pup grooming by the virgin female in LED-off and LED-on conditions. \*\* $P < 0.01$ , Mann-Whitney test with Bonferroni correction,  $n = 11$  animals for both GFP and ArchT groups. Error bars represent s.d. (see Supplementary Data for detailed statistics).

aggression and enhanced parenting, respectively. Furthermore, photoinactivation during pup exposure greatly reduced the later expression of anxiety-like behaviors (Fig. 4n), again indicating that acute responses of mPOA glutamatergic neurons to social stressors are required for the induction of anxiety-like behaviors.

In contrast to virgin males, virgin females exposed to a foreign pup did not have elevated anxiety-like behaviors (Extended Data Fig. 7d), consistent with photometry data showing that mPOA glutamatergic neurons in virgin females were not activated by interaction with pups (Fig. 4f). Nonetheless, optogenetic inactivation of mPOA glutamatergic neurons in virgin females reduced anxiety-like behaviors (Fig. 4o,p), regardless of pup exposure (Extended Data Fig. 7e). During pup exposure, neural inactivation greatly increased chances of pup retrieval (Fig. 4q) and prolonged the duration of pup grooming (Fig. 4r), indicating enhanced parenting. Together, these results support the notion that when the anxiety state is suppressed, social aggression is reduced, while parental behavior is promoted (in both sexes). Therefore, the mPOA-mediated emotional state is tightly linked to social behaviors.

It appears that silencing mPOA glutamatergic neurons can reduce anxiety-like behaviors even in animals unexposed to stressors (Extended Data Fig. 7e,f). We further examined basal-level anxiety-like behaviors using additional assays. Chemogenetic silencing of mPOA glutamatergic neurons reduced the time in shelter in an OFT (Extended Data Fig. 7g) as well as the time in the lit side in a dark-light box test<sup>30</sup> (Extended Data Fig. 7h). These results further support the notion that mPOA glutamatergic neurons also regulate basal-level anxiety-like behaviors.

**The mPOA-to-PAG pathway mediates anxiety-like behaviors.** We next explored downstream targets of the mPOA. Tracing axons from GFP-labeled mPOA glutamatergic neurons, we found that these cells projected strongly to the PAG, the lateral hypothalamic area and the superior mammillary body (Fig. 5a and Extended Data Fig. 8a). After photostimulating ChR2-expressing mPOA glutamatergic axons (at 15 Hz) in these target areas, we observed anxiety-like behaviors, such as jumping and aversion phenotypes, when the mPOA-to-PAG (but not to the lateral hypothalamic area or the superior mammillary body) pathway was activated (Extended Data Fig. 8b-d). We thus focused on the PAG. Injection of AAVretro-Cre into the PAG of Cre-dependent tdTomato reporter (Ai14) mice resulted in retrograde labeling of neurons in the mPOA (Fig. 5b). To further confirm the functional connectivity, we expressed ChR2 in mPOA glutamatergic neurons and made slice whole-cell recordings

from PAG neurons (Fig. 5c). With tetrodotoxin and 4-aminopyridine present in the bath solution, we observed LED-evoked monosynaptic excitatory postsynaptic currents (EPSCs) in recorded PAG neurons (Fig. 5d), confirming that PAG neurons receive direct excitatory input from the mPOA.

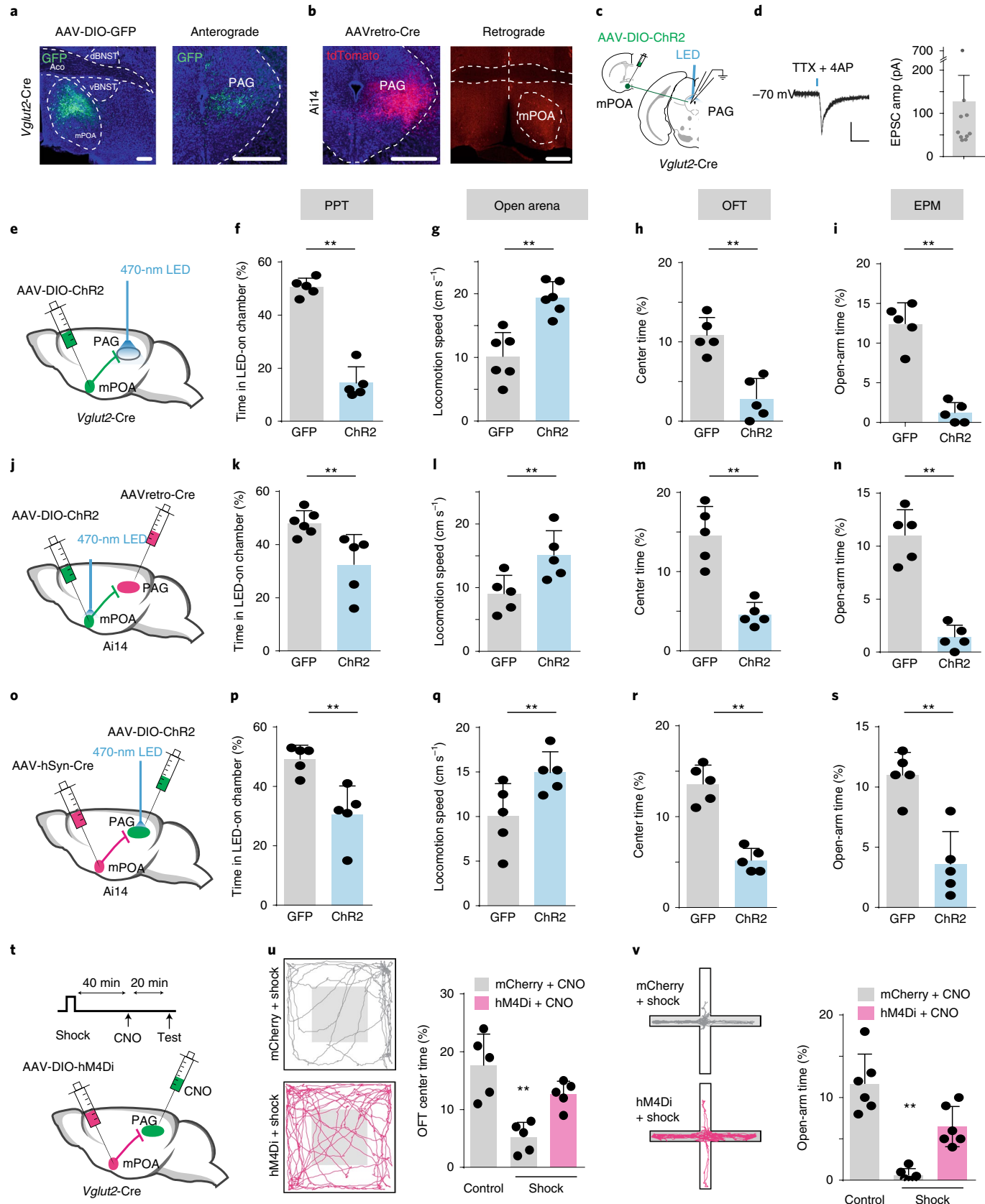
In freely moving mice, we specifically activated mPOA glutamatergic terminals in the PAG by implanting optic fibers above the PAG (Fig. 5e). LED stimulation reduced the time in the LED-on chamber in the PPT (Fig. 5f), consistent with the notion that these axons relay signals of negative valence. The stimulation also increased baseline locomotion in an open arena (Fig. 5g), as well as reduced center time in the OFT (Fig. 5h) and open-arm time in the EPM test (Fig. 5i), similar to the results obtained from stimulating the mPOA neurons per se. To further demonstrate the involvement of the mPOA→PAG pathway, we expressed ChR2 in PAG-projecting mPOA neurons by injecting AAVretro-Cre into the PAG and AAV encoding Cre-dependent ChR2 into the mPOA (Fig. 5j and Extended Data Fig. 8e). We also expressed ChR2 in mPOA-recipient PAG neurons by injecting AAV1-Cre into the mPOA and AAV encoding Cre-dependent ChR2 into the PAG<sup>31,32</sup> (Fig. 5o and Extended Data Fig. 8f). Optogenetic stimulation of PAG-projecting mPOA neurons or mPOA-recipient PAG neurons produced effects similar to stimulating mPOA→PAG axons: place avoidance (Fig. 5k,p), increased locomotion (Fig. 5l,q), reduced center time in the OFT (Fig. 5m,r) and reduced open-arm time in the EPM test (Fig. 5n,s). Additionally, we expressed hM4Di in mPOA glutamatergic neurons and injected CNO locally<sup>33</sup> into the PAG to specifically silence mPOA→PAG axon terminals (Fig. 5t). Again, this reduced anxiety-like behaviors after exposure to electric shocks (Fig. 5u,v). Together, these results suggest that the glutamatergic mPOA→PAG pathway can largely account for the role of the mPOA in regulating anxiety.

We further examined whether the glutamatergic mPOA→ventral tegmental area (VTA) pathway could be involved in regulating anxiety. Glutamatergic mPOA→VTA axons were relatively sparse (Extended Data Fig. 9a). Activation of these axons induced weak aversion phenotypes but did not affect anxiety-related behaviors (Extended Data Fig. 9b-d). Injections of cholera toxin subunit B (CTb) of different colors into the PAG and VTA, respectively, revealed that PAG- and VTA-projecting mPOA neurons were essentially separate neuronal populations (Extended Data Fig. 9e-g). Consistently, retrograde labeling of PAG-projecting mPOA neurons with AAVretro-Cre resulted in extremely sparse axon collaterals in the VTA (Extended Data Fig. 9h,i). These data indicate that our optogenetic stimulation

**Fig. 5 | The mPOA-to-PAG pathway primarily accounts for the role of the mPOA in regulating anxiety-like behaviors.** **a**, Representative images of GFP-labeled mPOA glutamatergic neurons (left) and their axons in the PAG (right). Scale bar, 500 μm. **b**, Retrograde labeling of neurons in the mPOA (right) by injection of AAVretro-Cre into the PAG (left). Scale bar, 500 μm. Aco, anterior commissure; dBNST, dorsal BNST; vBNST, ventral BNST. **c**, Photoactivation of mPOA glutamatergic axons and recording from PAG neurons in the slice preparation. **d**, Left: voltage-clamp recording from a PAG neuron showing a light-evoked EPSC. Right: average amplitudes (amp) of light-evoked EPSCs in recorded PAG neurons ( $n=10$ ). The error bar represents s.d. TTX, tetrodotoxin; 4AP, 4-aminopyridine. **e**, Photoactivation of mPOA glutamatergic axon terminals in the PAG. **f**, Percentage of time in the LED-on chamber in the PPT. \*\* $P < 0.01$ , two-sided Mann-Whitney test,  $n=5$  animals for both GFP and ChR2 groups. Error bars represent s.d. **g**, Average locomotion speed in an open arena. \*\* $P < 0.01$ , Mann-Whitney test,  $n=6$  animals for each group. Error bars represent s.d. **h**, Percentage of center time in the OFT. \*\* $P < 0.01$ , Mann-Whitney test,  $n=5$  animals for each group. Error bars represent s.d. **i**, Percentage of open-arm time in the EPM test. \*\* $P < 0.01$ , two-sided Mann-Whitney test,  $n=5$  animals for each group. Error bars represent s.d. **j**, Strategy for labeling PAG-projecting mPOA neurons with ChR2. **k-n**, As in **f-i**, for photoactivation of PAG-projecting mPOA neurons. \*\* $P < 0.01$ , two-sided Mann-Whitney test,  $n=5$  or  $n=6$  animals for each group. Error bars represent s.d. **o**, Strategy for photoactivation of mPOA-recipient PAG neurons. **p-s**, As in **f-i**, for photoactivation of mPOA-recipient PAG neurons. \*\* $P < 0.01$ , two-sided Mann-Whitney test,  $n=5$  or  $n=6$  animals for each group. Error bars represent s.d. **t**, Chemogenetic silencing of mPOA→PAG glutamatergic axon terminals and experimental timeline. **u**, Left: movement tracing for an example mCherry control (gray) and an hM4Di-expressing (red) animal in the OFT after exposure to electric shocks. Right: percentage of center times in the OFT for mCherry control animals in the control condition ( $n=5$ ), control animals after shocks ( $n=5$ ) and hM4Di-expressing animals after shocks ( $n=5$ ).  $P=0.0007$ , two-sided one-way ANOVA; \*\* $P < 0.01$ , post hoc test. Error bars represent s.d. **v**, Left: movement tracing for an mCherry control (gray) and an hM4Di-expressing animal (red) in the EPM test after exposure to shocks. Right: percentage of open-arm times in the EPM for mCherry control animals in the control condition ( $n=6$ ), control animals after shocks ( $n=6$ ) and hM4Di-expressing animals after shocks ( $n=6$ ).  $P < 0.0001$ , two-sided one-way ANOVA; \*\* $P < 0.01$ , post hoc test. Error bars represent s.d. Images in **a,b** are representative of  $n=6$  or  $n=3$  animals. (see Supplementary Data for detailed statistics).

of mPOA→PAG axon terminals is unlikely to affect mPOA→VTA axons and that mPOA glutamatergic neurons enhance anxiety-like behaviors primarily through their projection to the PAG.

**GABAergic mPOA neurons play opposing roles in regulating anxiety and parental behavior.** About half of mPOA neurons are GABAergic<sup>34</sup>. Using *Slc32a1-Cre* (*Vgat-Cre*) mice, we next



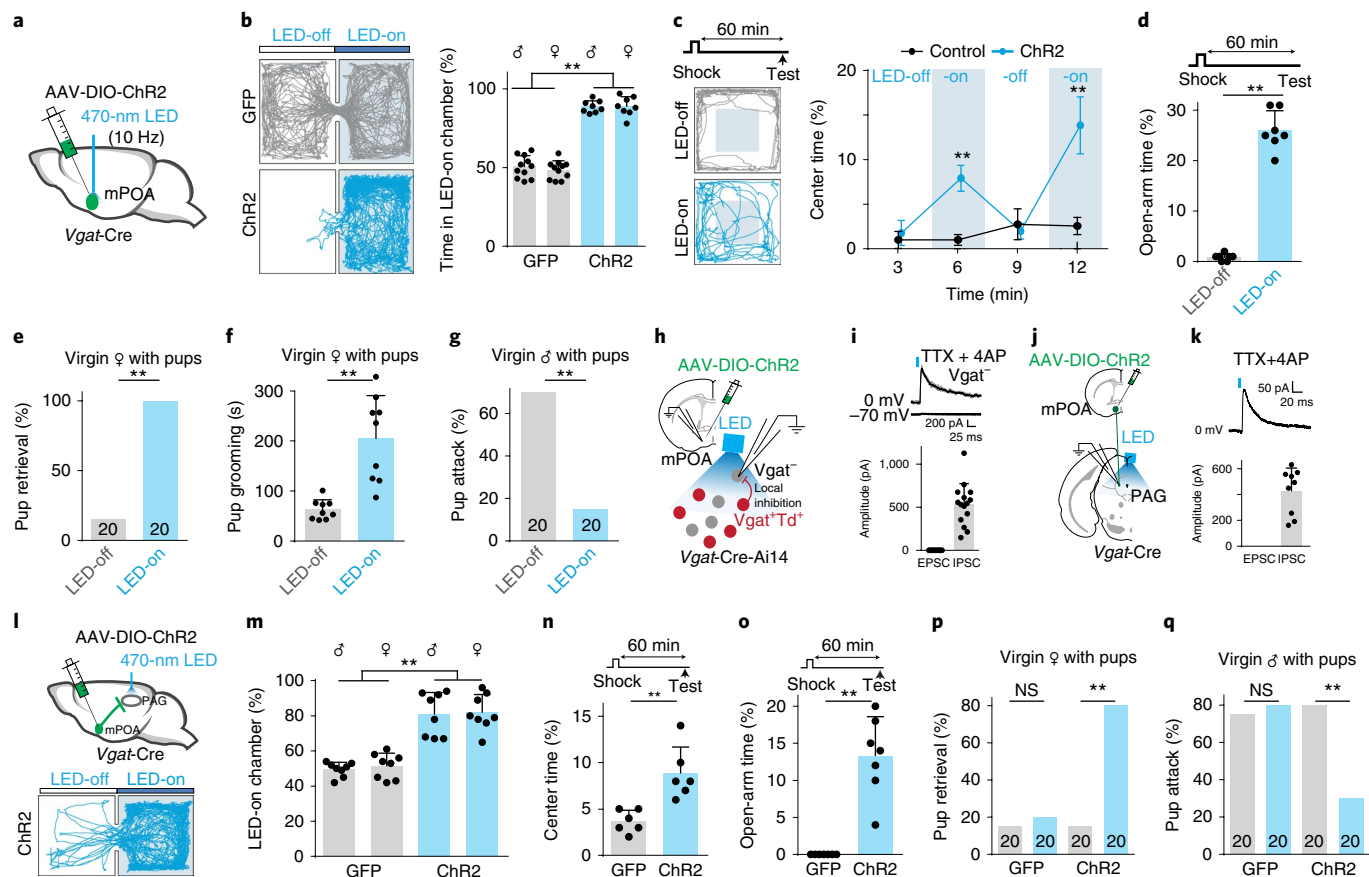


**Fig. 6 | GABAergic neurons play opposing roles in regulating anxiety state and parental behavior.** **a**, Expressing ChR2 in mPOA GABAergic neurons. **b**, Left: representative movement tracing of a GFP control (gray) and a ChR2-expressing (blue) animal in the PPT. Right: percentage of time in the LED-on chamber for GFP ( $n=11$  males and 11 females) and ChR2-expressing ( $n=8$  males and 8 females) mice. \*\* $P < 0.01$ , one-way repeated-measures ANOVA. Error bars represent s.d. **c**, Left: movement tracing for a ChR2-expressing animal in the OFT in an LED-off (gray) and an LED-on (blue) block. Right: percentage of center times for GFP control (black) and ChR2-expressing (blue) animals in LED-off and LED-on blocks. \*\* $P < 0.01$ , two-way repeated-measures ANOVA test,  $n=7$  animals (four males) for each group. Error bars represent s.d. **d**, Percentage of open-arm times for ChR2-expressing animals ( $n=7$ ; four males) in LED-off and LED-on conditions. \*\* $P < 0.01$ , two-sided Mann-Whitney test. Error bars represent s.d. **e**, Percentage of trials with the virgin female exhibiting pup retrieval in LED-on and LED-off conditions. \*\* $P < 0.01$ , two-sided Fisher's exact test with Bonferroni correction,  $n=7$  ChR2-expressing animals. **f**, Duration of pup grooming by the virgin female in LED-off and LED-on conditions. \*\* $P < 0.01$ , two-sided Mann-Whitney test with Bonferroni correction,  $n=9$  ChR2-expressing animals. Error bars represent s.d. **g**, Percentage of trials with virgin males attacking the pup in LED-off and LED-on conditions. \*\* $P < 0.01$ , two-sided Fisher's exact test with Bonferroni correction,  $n=7$  ChR2-expressing animals. **h**, Recording from mPOA Vgat<sup>+</sup> neurons while stimulating Vgat<sup>+</sup> neurons in the slice preparation. **i**, Top: traces of voltage-clamp recording from an mPOA glutamatergic neuron under two holding potentials. The vertical blue line indicates the onset of light stimulation. Bottom: average amplitudes of EPSCs and IPSCs in 15 mPOA glutamatergic neurons. Error bars represent s.d. **j**, Recording from PAG neurons and photostimulation of ChR2-expressing GABAergic mPOA axons. **k**, Top: a light-evoked IPSC recorded in a PAG neuron. Bottom: average amplitudes of EPSCs and IPSCs from nine PAG neurons. Error bars represent s.d. **l**, Top: stimulation of GABAergic mPOA axons in the PAG. Bottom: movement tracing for an example animal in the PPT. **m**, Right: percentage of time in the LED-on chamber for GFP control and ChR2-expressing animals. \*\* $P < 0.01$ , two-sided, two-way repeated-measures ANOVA,  $n=8$  animals for each group. Error bars represent s.d. **n**, Percentage of center times in the OFT for GFP control and ChR2-expressing animals. \*\* $P < 0.01$ , two-sided Mann-Whitney test,  $n=6$  animals (three males) for each group. Error bars represent s.d. **o**, Percentage of open-arm times in the EPM test for GFP control and ChR2-expressing animals. \*\* $P < 0.01$ , two-sided Mann-Whitney test,  $n=7$  animals (four males) for each group. Error bars represent s.d. **p**, Percentage of trials with the virgin female exhibiting pup retrieval in LED-off (gray) and LED-on (blue) conditions. \*\* $P < 0.01$ , two-sided Fisher's exact test with Bonferroni correction,  $n=8$  animals for both GFP and ChR2 groups. **q**, Percentage of trials with the virgin male attacking the pup in LED-off and LED-on conditions. \*\* $P < 0.01$ , two-sided Fisher's exact test with Bonferroni correction,  $n=8$  animals for both GFP and ChR2 groups (see Supplementary Data for detailed statistics).

examined whether GABAergic neurons also played a role in regulating anxiety-like behaviors. Stimulating GABAergic mPOA neurons (Fig. 6a) produced strong place preference (that is, positive valence) in both males and females (Fig. 6b) and reversibly increased the center time in the OFT (Fig. 6c) as well as increased the open-arm time in the EPM test (Fig. 6d). Activation of these neurons also enhanced parental behaviors in virgin females (Fig. 6e,f), while reducing pup-directed aggression in virgin males (Fig. 6g). No effect was observed in GFP control mice (Extended Data Fig. 10a–e). Thus,

GABAergic and glutamatergic mPOA neurons play opposite roles in regulating both anxiety-like and parental behaviors.

We next explored intra-mPOA connectivity by specifically expressing ChR2 in mPOA GABAergic neurons in *Vgat-Cre-Ai14* mice. As Vglut2<sup>+</sup> and Vgat<sup>+</sup> neurons are separate populations and together cover almost all the neurons in the mPOA<sup>34</sup>, we were able to selectively record from glutamatergic neurons in slice preparations while optically stimulating GABAergic neurons (Fig. 6h). Strong light-evoked monosynaptic inhibitory postsynaptic currents

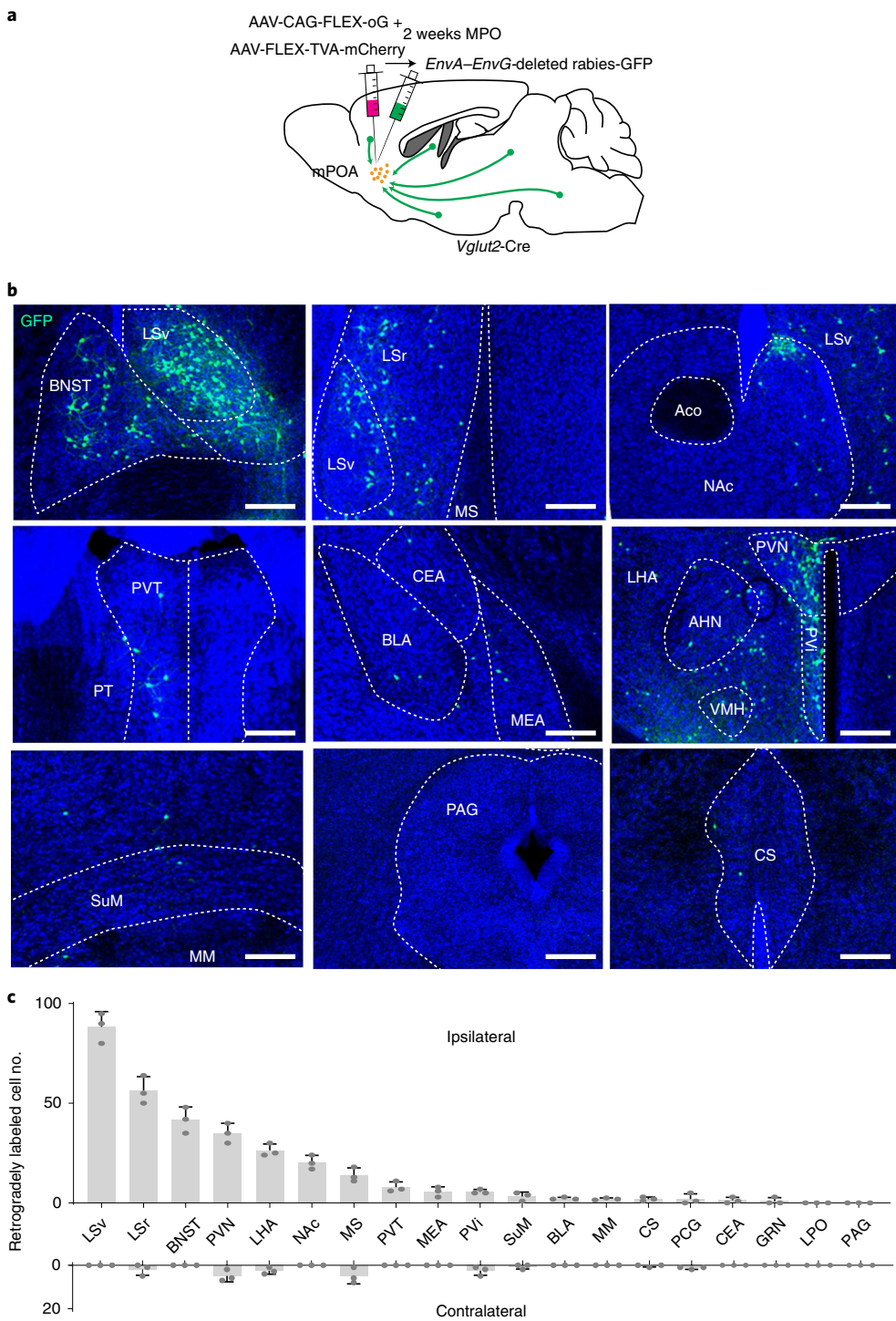


**Fig. 7 | Monosynaptic inputs to mPOA glutamatergic neurons.** **a**, Strategy for cell-type-specific tracing of monosynaptic inputs using pseudotyped rabies. **b**, Example images of retrogradely labeled neurons in different brain regions. Scale bar, 500 μm. LSV, ventral LS; LSr, rostral LS; MS, medial septum; NAc, nucleus accumbens; aco, anterior commissure; PVT, periventricular nucleus of the thalamus; PT, paratenial nucleus; BLA, basolateral amygdala; CEA, central amygdala; MEA, medial amygdala; AHN, anterior hypothalamic nucleus; VMH, ventromedial hypothalamic nucleus; PVN, periventricular hypothalamic nucleus; SuM, supramammillary nucleus; MM, mammillary nucleus; CS, superior central nucleus raphe; LHA, lateral hypothalamic area. **c**, Quantification of numbers of retrogradely labeled cells in different regions in contralateral and ipsilateral sides of the injected mPOA ( $n=3$  animals, error bars represent s.d.). PCG, pontine central gray; GRN, gigantocellular reticular nucleus; LPO, lateral preoptic area. Images in **b** are representative of  $n=3$  animals.

(IPSCs) were observed (Fig. 6*i*), indicating that GABAergic neurons can suppress glutamatergic neurons locally.

Slice recording revealed that GABAergic neurons provided direct inhibitory input to PAG neurons (Fig. 6*j,k*). We then tested

the functional impact of this long-range inhibitory projection. Photostimulation of GABAergic mPOA→PAG terminals (Extended Data Fig. 10*f*) produced place preference (Fig. 6*l,m*), reduced anxiety-like behaviors (Fig. 6*n,o*), enhanced parental behavior in

females (Fig. 6p) and reduced pup-directed aggression in males (Fig. 6q). Therefore, mPOA GABAergic neurons regulate both anxiety-like and parental behaviors in a manner antagonistic to glutamatergic neurons not only by locally inhibiting glutamatergic neurons but also by sending a competing (that is, inhibitory) projection to the PAG.

**Inputs to mPOA glutamatergic neurons.** What are input sources to mPOA glutamatergic neurons? To address this question, we applied cell-type-specific retrograde tracing of monosynaptic inputs using pseudotyped rabies virus<sup>35</sup> (Fig. 7a). Retrogradely labeled cells were observed in a number of regions, in particular the LS, BNST and PVN (Fig. 7b,c). The latter structures were all previously implicated in anxiety or stress responses<sup>1,3,36–39</sup>. In general, these identified input structures are consistent with previous anatomical results<sup>40</sup> and suggest that mPOA neurons may integrate aversive event information from multiple sources.

## Discussion

In the present study, we found that mPOA glutamatergic neurons are activated by exposure to anxiogenic stressors and that their baseline firing rates are increased for a long period of time after exposure. Cell-type specific examination revealed opposite roles of mPOA glutamatergic and GABAergic neurons in regulating anxiety-like behaviors: glutamatergic neurons enhance anxiety-like behaviors and mediate stress-induced anxiety states, whereas GABAergic neurons suppress anxiety-like behaviors. GABAergic neurons antagonize the effects of glutamatergic neurons not only by locally inhibiting the latter but also by sending a parallel but competing projection to the common target, the PAG. In addition, these two neuronal populations both antagonistically coordinate anxiety-like and parental behaviors: they enhance anxiety-like behaviors while reducing parental behaviors and vice versa. These results implicate the mPOA in the anxiety-related network. In particular, the mPOA may play an important role in coordinating emotional state and social behavior.

**mPOA glutamatergic neurons generally modulate anxiety states.** Although the mPOA was previously implicated in a variety of fundamental functions, including sleep, hunting, mating and parenting<sup>15,18–20,41,42</sup>, these functional roles were mostly attributed to its GABAergic populations expressing differential molecular markers besides GABA<sup>34</sup>. The functional role of its glutamatergic population has yet remained unclear. Here, our results indicate that the mPOA serves as a critical center to regulate anxiety states through its glutamatergic neurons. Activating these cells can directly trigger anxiety-like behaviors, while silencing them alleviates the expression of anxiety-like behaviors after exposure to a variety of physical and social stressors. While these effects were observed in both sexes under our experimental conditions, we do not exclude any possibilities of sex differences (for example, different activation thresholds for the induction of anxiety-like behaviors). The baseline firing rates of these neurons are increased for a relatively long period of time after stress exposure, which accounts for the persistence of the induced anxiety state. In addition, suppressing the baseline activity of these neurons is sufficient to reduce basal-level anxiety-like behaviors. Furthermore, their activity during exposure to stressors is required for and promotes the induction of an anxiety state. Together, our results demonstrate that mPOA glutamatergic neurons regulate the induction, expression and maintenance of anxiety states in general.

Our additional experiments indicate that mPOA glutamatergic neurons are not involved in hunting-like behaviors or thermal regulation (Extended Data Fig. 10g–i), functions that were reported for a different molecularly defined cell group (CaM kinase (CaMK) II $\alpha^+$ ) in the mPOA and glutamatergic neurons in a spatially close

nucleus (ventral lateral preoptic area) of the preoptic area, respectively<sup>41,43</sup>. This excludes the possibility that the elevated anxiety state resulting from the activation of mPOA glutamatergic neurons is due to a side effect of changes in body temperature. On the other hand, the elevated anxiety state is in line with the observed increase in wakefulness<sup>42</sup>, as anxiety disorders are often accompanied by sleep problems<sup>44</sup>.

mPOA glutamatergic neurons likely receive information about aversive cues and/or events from multiple sources, including the LS, BNST and PVN (Fig. 7). Neurons of these structures were shown to respond to aversive stimuli<sup>8,10,36</sup>. Therefore, mPOA glutamatergic neurons may be able to integrate multiple types of information to potently regulate anxiety states under diverse sensory and social contexts. Multiple mechanisms may underlie the enhanced baseline activity of these neurons after stress exposure: increases in the synaptic strength of their inputs, in the intrinsic excitability of these neurons per se and/or in the spiking activity of any of their input structures. In other words, ‘stress memory’ may be stored locally within the mPOA or remotely in its upstream structures.

**mPOA glutamatergic neurons can encode extremely negative valence.** Regulation of negative emotions, including fear and anxiety, depends on the processing of negative valence<sup>1,3,45</sup>. Compared to previously studied structures, such as the BNST<sup>8</sup> and the PVN<sup>36</sup>, activation of mPOA glutamatergic neurons appears to result in an extremely strong negative emotion. Noticeably, in PPTs, the percentage of time spent in the photostimulation chamber (Fig. 2e) is less than that when other structures are activated<sup>8,36</sup>, and animals exhibit frequent rearing and jumping behaviors when placed in an inescapable context (Extended Data Fig. 6d–g). More strikingly, in conflict tests, animals prefer to stay in places where physical harm could be inflicted rather than in those only associated with photostimulation (Extended Data Fig. 6a–c). These results provide strong evidence that activity of mPOA glutamatergic neurons can encode extremely negative valence and thus may lead to a severely anxious state. This property of mPOA glutamatergic neurons suggests that they might be a unique therapeutic target for treating severe anxiety disorders.

**An opposite role of mPOA GABAergic neurons.** Opposite to glutamatergic neurons, our results demonstrate that mPOA GABAergic neurons, as a whole population, encode positive valence and promote parental behavior. This is consistent with observations in previous studies on molecularly identified subpopulations of GABAergic neurons in the mPOA<sup>15,18–20,34</sup>. For example, both galanin (Gal)<sup>+</sup> and estrogen receptor (Esr)<sup>1+</sup> mPOA neurons promote rewarding phenotypes and parental behavior<sup>18,19</sup>, and neurotensin (Nts)<sup>+</sup> mPOA neurons encode attractive male cues and promote social approach in females<sup>20</sup>. Notably, by comparing glutamatergic and GABAergic neurons, our current study reveals that the rewarding phenotype (that is, place preference) induced by activating GABAergic neurons is much stronger than that resulting from silencing the glutamatergic neurons themselves (compare Fig. 6b and Extended Data Fig. 6l–n). This further indicates that the activity of glutamatergic neurons cannot encode a full spectrum of valence values and that positive valence is mainly coded by GABAergic neurons. Besides valence coding, our study further reveals that activity of GABAergic neurons is strongly anxiolytic, as activation of these neurons greatly suppresses anxiety-like behaviors and social aggression. It is likely that rewarding social cues can directly generate anxiolytic effects, by activating mPOA GABAergic neurons<sup>19,20</sup>. Our results suggest that targeting mPOA GABAergic neurons might be another powerful therapeutic strategy for anxiety disorders.

**Antagonistic control of anxiety state and parenting by mPOA neurons.** Previously, an antagonistic relationship between anxiety- and parenting-related behaviors was documented: enhanced anxiety

is known to suppress parental behavior<sup>46</sup>, while reduced anxiety was observed in postpartum animals that show elevated parental behavior<sup>47,48</sup>. In the present study, the finding that manipulating mPOA neurons affects both parenting and anxiety levels demonstrates that the mPOA plays a critical role in coordinating the anxiety state and parental behavior. Such coordination is likely achieved through competitive interactions between glutamatergic and GABAergic neurons: GABAergic neurons locally inhibit glutamatergic neurons and compete with the latter through their long-range inhibitory projections to the common target, the PAG, which is implicated in providing motor commands for parental behavior<sup>49</sup>. While glutamate neurons promote an anxiety state, and GABA neurons promote parental behaviors, coordinating the relative activity in the two populations determines which type of behavior is expressed (Extended Data Fig. 10o). It is also possible that glutamatergic neurons suppress parental behaviors in an indirect manner, as promoting anxiety can nonspecifically suppress affiliative behavior. Additional retrograde labeling experiments suggest that about two-thirds of PAG-projecting mPOA neurons are glutamatergic, while about one-third of these are GABAergic (Extended Data Fig. 10j–n). This provides an explanation for the result that activating PAG-projecting mPOA neurons as a population produces a similar but weaker effect than activating mPOA glutamatergic axons in the PAG (compare Fig. 5f,k).

**Functional relationship between the mPOA and the BNST.** A spatially proximate nucleus, the BNST, was previously implicated in physical stress-related anxiety<sup>8</sup>. In particular, glutamatergic and GABAergic neurons in the ventral BNST were shown to encode opposing motivational states and produce anxiogenic and anxiolytic behavioral phenotypes, respectively<sup>8,39</sup>. The mPOA and ventral BNST can be clearly distinguished based on their differences in anatomical characteristics (for example, input and output organization)<sup>40,50</sup> as well as on distributions of molecularly identified cell types<sup>34,40</sup> (Extended Data Fig. 1f,g). Considering that the mPOA receives axonal projections unidirectionally from the BNST (Extended Data Fig. 4a), it is possible that the two structures may play some similar functional roles in regulating physical stress-induced anxiety. However, as they have different input and output connectivity patterns, the two structures may also exhibit distinct functional roles under different sensory and behavioral contexts. We speculate that the mPOA may play a more unique role in mediating socially induced anxiety states.

In summary, we identified the mPOA as a previously unrecognized structure that controls anxiety state and mediates the induction and expression of stress-induced anxiety-like behaviors. We propose that activity of mPOA glutamatergic and GABAergic neurons is highly correlated with the value of negative and positive valences, respectively. The balance between activities of these neurons through competitive interactions may thus allow the expression of emotional state under different sensory and social contexts with a broad dynamic range.

## Online content

Any methods, additional references, Nature Research reporting summaries, source data, extended data, supplementary information, acknowledgements, peer review information; details of author contributions and competing interests; and statements of data and code availability are available at <https://doi.org/10.1038/s41593-020-00784-3>.

Received: 26 January 2020; Accepted: 18 December 2020;  
Published online: 1 February 2021

## References

- Calhoon, G. G. & Tye, K. M. Resolving the neural circuits of anxiety. *Nat. Neurosci.* **18**, 1394–1404 (2015).
- Craske, M. G. & Stein, M. B. Anxiety. *Lancet* **388**, 3048–3059 (2016).
- Tovote, P., Fadok, J. P. & Lüthi, A. Neuronal circuits for fear and anxiety. *Nat. Rev. Neurosci.* **16**, 317–331 (2015).
- Fenster, R. J., Lebois, L. A. M., Ressler, K. J. & Suh, J. Brain circuit dysfunction in post-traumatic stress disorder: from mouse to man. *Nat. Rev. Neurosci.* **19**, 535–551 (2018).
- Merikangas, K. R. et al. Longitudinal trajectories of depression and anxiety in a prospective community study: the Zurich Cohort Study. *Arch. Gen. Psychiatry* **60**, 993–1000 (2003).
- Adhikari, A. Distributed circuits underlying anxiety. *Front. Behav. Neurosci.* **8**, 112 (2014).
- Tye, K. M. et al. Amygdala circuitry mediating reversible and bidirectional control of anxiety. *Nature* **471**, 358–362 (2011).
- Jennings, J. H. et al. Distinct extended amygdala circuits for divergent motivational states. *Nature* **496**, 224–228 (2013).
- Kim, S. Y. et al. Diverging neural pathways assemble a behavioural state from separable features in anxiety. *Nature* **496**, 219–223 (2013).
- Anthony, T. E. et al. Control of stress-induced persistent anxiety by an extra-amygdala septohypothalamic circuit. *Cell* **156**, 522–536 (2014).
- Padilla-Coreano, N. et al. Hippocampal-prefrontal theta transmission regulates avoidance behavior. *Neuron* **104**, 601–610 (2019).
- Felix-Ortiz, A. C., Burgos-Robles, A., Bhagat, N. D., Leppla, C. A. & Tye, K. M. Bidirectional modulation of anxiety-related and social behaviors by amygdala projections to the medial prefrontal cortex. *Neuroscience* **321**, 197–209 (2016).
- Adhikari, A., Topiwala, M. A. & Gordon, J. A. Synchronized activity between the ventral hippocampus and the medial prefrontal cortex during anxiety. *Neuron* **65**, 257–269 (2010).
- Wichmann, R. et al. Acute stress induces long-lasting alterations in the dopaminergic system of female mice. Preprint at *bioRxiv* <https://doi.org/10.1101/168492> (2017).
- Wei, Y. C. et al. Medial preoptic area in mice is capable of mediating sexually dimorphic behaviors regardless of gender. *Nat. Commun.* **9**, 279 (2018).
- Xu, X. et al. Modular genetic control of sexually dimorphic behaviors. *Cell* **148**, 596–607 (2012).
- Dulac, C., O'Connell, L. A. & Wu, Z. Neural control of maternal and paternal behaviors. *Science* **345**, 765–770 (2014).
- Fang, Y. Y., Yamaguchi, T., Song, S. C., Tritsch, N. X. & Lin, D. A hypothalamic midbrain pathway essential for driving maternal behaviors. *Neuron* **98**, 192–207 (2018).
- Wu, Z., Autry, A. E., Bergan, J. F., Watabe-Uchida, M. & Dulac, C. G. Galanin neurons in the medial preoptic area govern parental behaviour. *Nature* **509**, 325–330 (2014).
- McHenry, J. A. et al. Hormonal gain control of a medial preoptic area social reward circuit. *Nat. Neurosci.* **20**, 449–458 (2017).
- Carola, V., D'Olimpio, F., Brunamonti, E., Mangia, F. & Renzi, P. Evaluation of the elevated plus-maze and open-field tests for the assessment of anxiety-related behaviour in inbred mice. *Behav. Brain Res.* **134**, 49–57 (2002).
- Ahrens, S. et al. A central extended amygdala circuit that modulates anxiety. *J. Neurosci.* **38**, 5567–5583 (2018).
- Xiu, J. et al. Visualizing an emotional valence map in the limbic forebrain by TAI-FISH. *Nat. Neurosci.* **17**, 1552–1559 (2014).
- Luo, L., Callaway, E. M. & Svoboda, K. Genetic dissection of neural circuits: a decade of progress. *Neuron* **98**, 256–281 (2018).
- Liu, Z. et al. Dorsal raphe neurons signal reward through 5-HT and glutamate. *Neuron* **81**, 1360–1374 (2014).
- Hu, H. Reward and aversion. *Annu. Rev. Neurosci.* **39**, 297–324 (2016).
- Zhang, G. W. et al. Transforming sensory cues into aversive emotion via septal-habenular pathway. *Neuron* **99**, 1016–1028 (2018).
- Breton-Provencher, V. & Sur, M. Active control of arousal by a locus coeruleus GABAergic circuit. *Nat. Neurosci.* **22**, 218–228 (2019).
- Neumann, I. D., Veenema, A. H. & Beiderbeck, D. I. Aggression and anxiety: social context and neurobiological links. *Front. Behav. Neurosci.* **4**, 12 (2010).
- Bluett, R. J. et al. Central anandamide deficiency predicts stress-induced anxiety: behavioral reversal through endocannabinoid augmentation. *Transl. Psychiatry* **4**, e408 (2014).
- Wang, L. et al. The coding of valence and identity in the mammalian taste system. *Nature* **558**, 127–131 (2018).
- Zingg, B. et al. AAV-mediated anterograde transsynaptic tagging: mapping corticocollicular input-defined neural pathways for defense behaviors. *Neuron* **93**, 33–47 (2017).
- Zhu, Y., Wienecke, C. F. R., Nachtrab, G. & Chen, X. A thalamic input to the nucleus accumbens mediates opiate dependence. *Nature* **530**, 219–222 (2016).
- Moffitt, J. R. et al. Molecular, spatial, and functional single-cell profiling of the hypothalamic preoptic region. *Science* **362**, eaau5324 (2018).
- Callaway, E. M. & Luo, L. Monosynaptic circuit tracing with glycoprotein-deleted rabies viruses. *J. Neurosci.* **35**, 8979–8985 (2015).

36. Kim, J. et al. Rapid, biphasic CRF neuronal responses encode positive and negative valence. *Nat. Neurosci.* **22**, 576–585 (2019).
37. Davis, M., Walker, D. L., Miles, L. & Grillon, C. Phasic vs sustained fear in rats and humans: role of the extended amygdala in fear vs anxiety. *Neuropsychopharmacology* **35**, 105–135 (2010).
38. Parfitt, G. M. et al. Bidirectional control of anxiety-related behaviors in mice: role of inputs arising from the ventral hippocampus to the lateral septum and medial prefrontal cortex. *Neuropsychopharmacology* **42**, 1715–1728 (2017).
39. McHenry, J. A., Rubinow, D. R. & Stuber, G. D. Maternally responsive neurons in the bed nucleus of the stria terminalis and medial preoptic area: putative circuits for regulating anxiety and reward. *Front. Neuroendocrinol.* **38**, 65–72 (2015).
40. Oh, S. W. et al. A mesoscale connectome of the mouse brain. *Nature* **508**, 207–214 (2014).
41. Park, S. G. et al. Medial preoptic circuit induces hunting-like actions to target objects and prey. *Nat. Neurosci.* **21**, 364–372 (2018).
42. Chung, S. et al. Identification of preoptic sleep neurons using retrograde labelling and gene profiling. *Nature* **545**, 477–481 (2017).
43. Zhao, Z. D. et al. A hypothalamic circuit that controls body temperature. *Proc. Natl Acad. Sci. USA* **114**, 2042–2047 (2017).
44. Papadimitriou, G. N. & Linkowski, P. Sleep disturbance in anxiety disorders. *Int. Rev. Psychiatry* **17**, 229–236 (2005).
45. Tye, K. M. Neural circuit motifs in valence processing. *Neuron* **100**, 436–452 (2018).
46. Glasheen, C., Richardson, G. A. & Fabio, A. A systematic review of the effects of postnatal maternal anxiety on children. *Arch. Women's Ment. Health* **13**, 61–74 (2010).
47. Hård, E. & Hansen, S. Reduced fearfulness in the lactating rat. *Physiol. Behav.* **35**, 641–643 (1985).
48. Lonstein, J. S. Regulation of anxiety during the postpartum period. *Front. Neuroendocrinol.* **28**, 115–141 (2007).
49. Kohl, J. et al. Functional circuit architecture underlying parental behaviour. *Nature* **556**, 326–331 (2018).
50. Dong, H. W., Petrovich, G. D. & Swanson, L. W. Topography of projections from amygdala to bed nuclei of the stria terminalis. *Brain Res. Rev.* **38**, 192–246 (2001).

**Publisher's note** Springer Nature remains neutral with regard to jurisdictional claims in published maps and institutional affiliations.

© The Author(s), under exclusive licence to Springer Nature America, Inc. 2021

## Methods

Animal experiments were conducted in accordance with guidelines for the care and use of laboratory animals from the US National Institutes of Health and under protocols approved by the Institutional Animal Care and Use Committee at the University of Southern California and Southern Medical University.

**Animals.** *Vglut2*-ires-Cre (016963), *Vgat*-ires-Cre (016962), Ai14 (Cre-dependent tdTomato reporter line, 007914), Ai27 (Cre-dependent ChR2 reporter line, 012567), Ai75 (Cre-dependent nuclear-localized tdTomato reporter line, 025106), *Dat*-ires-Cre (006660) and C57BL/6 mice were obtained from Jackson Laboratory. Mice were housed at 18–23°C with 40–60% humidity in a 12-h light–dark cycle with ad libitum access to food and water. Experiments were performed on adult male and female mice (6–12 weeks old) during the dark cycle. Regarding animal cohorts, in general, a cohort of mice was subjected to a battery of anxiety-like behavioral assays, with gaps of at least 72 h, to reduce the total number of animals used. However, animals in a cohort did not necessarily undergo the same number of tests due to changes in animal conditions (for example, broken optical cannula). Separate groups of mice were used for different control treatments in Fig. 1c. In Fig. 2, separate cohorts were used for the valence test and anxiety-like behavior tests.

**Viruses.** AAV2/1-pEF1a-DIO-hChR2-eYFP ( $1.82 \times 10^1$  genome copies (GC) ml $^{-1}$ , UPenn vector core), AAV1-CAG-FLEX-GFP-WPRE ( $2 \times 10^{13}$  GC ml $^{-1}$ , UPenn vector core, Addgene, 51502), AAVRetro-Cre ( $1.5 \times 10^{14}$  GC ml $^{-1}$ , Vigene<sup>®</sup>), AAV1-CAG-FLEX-ArchT-GFP ( $4 \times 10^{12}$  GC ml $^{-1}$ , UNC vector core), pAAV-hSyn-DIO-hM4D(Gq)-mCherry ( $1.3 \times 10^{13}$  GC ml $^{-1}$ , Addgene, 44361), pAAV-hSyn-DIO-hM4D(Gi)-mCherry ( $3 \times 10^{13}$  GC ml $^{-1}$ , Addgene, 44362), pAAV-hSyn-DIO-mCherry ( $4.8 \times 10^{13}$  GC ml $^{-1}$ , Addgene, 50459), AAV1-Syn-FLEX-GCamp6s-WPRE-SV4 (Addgene, 100845), AAV1-DIO-FLPo-WPRE-hGHPa ( $1.53 \times 10^{14}$  GC ml $^{-1}$ , Addgene, 87306), AAV8-CAG-fDIO-TVA-mCherry ( $1.1 \times 10^{13}$  GC ml $^{-1}$ , Salk Institute), AAV<sub>DJ</sub>-CAG-fDIO-oG-WPRE ( $4.4 \times 10^{13}$  GC ml $^{-1}$ , Salk Institute) and *EnvA*-*EnvG*-deleted rabies-GFP ( $8.13 \times 10^8$  GC ml $^{-1}$ , Salk Institute) were used in this study. The volume for each injection was 50 nl.

**Surgical procedures.** Mice were anesthetized with 1.5–2% isoflurane. A small cut was made on the skin covering the craniotomy position, and the muscles were removed. One ~0.25-mm $^2$  craniotomy window was made for each region. AAVs (encoding ChR2, ArchT, hM4D(Gi), hM4D(Gq), GFP, mCherry, GCamp6s) were used, depending on the purpose of the experiment and the strain of mice. A beveled glass micropipette (pulled using Model P-97, Sutter Instrument; tip diameter, 10–20  $\mu$ m) was used to deliver the virus. Virus was delivered by either pressure injection or iontophoresis, and the glass micropipette was attached to a microsyringe pump (World Precision Instruments). For pressure injection, 50 nl of the viral solution was injected at a rate of 15 nl min $^{-1}$ . For iontophoresis injection, a current was applied (3  $\mu$ A, cycle of 7 s on, 7 s off) for 5 min. After the injection, the pipette was allowed to rest for 5 min before withdrawal. The scalp was then sutured. Following surgery, 0.1 mg per kg buprenorphine was injected subcutaneously before returning the animals to their home cages. Mice were allowed to recover for at least 2 weeks before cannula implantation, behavioral tests or recording experiments. After each experiment, the brain was sectioned and automatically imaged under a confocal microscope to confirm viral expression. Image tiles were online stitched (FluoView FV1000, Olympus).

For optogenetic manipulations, animals were anesthetized with isoflurane, and an optic cannula (400  $\mu$ m, Thorlabs) was stereotactically implanted into the targeted region depending on the purpose of the experiment (mPOA, bilateral implantation, anterior–posterior (AP) +0.9 mm, medial–lateral (ML) +1.3 mm, dorsal–ventral (DV) –4.75 mm, with a 10° angle; PAG, bilateral implantation, AP –4.4 mm, ML +1.5 mm, DV –2.2 mm; ventral lateral preoptic area, bilateral implantation, AP +0.9 mm, ML +2 mm, DV –5.2 mm, with a 10° angle; median preoptic area, unilateral implantation, AP +1.5 mm, ML +0.2 mm, DV –4.4 mm on a 10° posterior angle; VTA, bilateral implantation, AP –3.28 mm, ML 0.4 mm, DV –4.1 mm). The optic cannula was fixed with dental cement. The mice were allowed to recover for at least 1 week before the behavior tests. After each experiment, the brain was sectioned and imaged under a confocal microscope to confirm locations of viral expression and the implantation site. For pharmacological manipulations, animals were anesthetized with isoflurane, and a drug cannula (RWD; internal diameter, 140  $\mu$ m) was stereotactically implanted into the target region based on the purpose of the experiment.

**In vivo optogenetic stimulation.** During the 3 d before behavioral tests, animals were attached to optical fibers without LED stimulation for habituation. On the test day, the optic fiber (200- $\mu$ m core, 0.22 numerical aperture (NA), Thorlabs) was connected to a blue LED source (480 nm, pulses of 0–30 Hz, 5-ms pulse duration, Thorlabs) for stimulation, or a green LED source (530 nm, constant illumination as described for each behavioral test). The LED power measured at the tip of the fiber (connected with the optic cannula) was approximately 3–5 mW. The LED stimulation frequency of blue light was 10 Hz for most experiments, which is within the physiological range of firing rates of *Vglut2* neurons in the mPOA.

Repeated LED-on and LED-off epochs were applied for Figs. 2j, 3j and 6c. For Fig. 2j, pupil size data were averaged over trials for each animal. For Figs. 3j and 6c, only one test session was performed on each animal, and data for each individual epoch were averaged for all animals.

**In vivo chemogenetic manipulation.** For DREADD experiments, animals expressing hM4D(Gi) or hM3D(Gq) received either an intraperitoneal injection of CNO (1 mg per kg) or a local infusion of CNO (5  $\mu$ M, 150 nl) through the implanted cannula to the targeted region.

**Fiber photometry recording.** To obtain calcium signals, LED light (480 nm, Thorlabs) was bandpass filtered (ET470/24M, Chroma), focused by an objective lens (Olympus) and coupled to an optical fiber (O.D. = 400  $\mu$ m, NA = 0.48, 1 m long, Doric). The fiber was connected to the implanted optic fiber (400  $\mu$ m, NA = 0.5, Thorlabs) using a ceramic sleeve. The LED power was adjusted to 0.02 mW at the tip of the optical fiber. At this power, no significant photobleaching was observed. The fluorescent calcium signal was bandpass filtered (ET525/36M, Chroma) and collected by a photomultiplier tube (H11706-40, Hamamatsu) and then passed through an amplifier (Model SR570, Stanford Research System) and low-pass filtered (30 Hz). The current signal was converted to a voltage signal using a data acquisition card (PCI-MIO-16E-4, National Instruments) and digitized at 250 Hz. Data were obtained using custom LabVIEW software and analyzed offline using custom MATLAB software. No movement-related artifact was detected by our system.

**Electrophysiological recording and spike sorting.** Multichannel recording was carried out with a 16-channel silicone probe (A1x16-Poly2-5mm-50s-177-A16, 16 contacts separated by 50  $\mu$ m, NeuroNexus Technologies). Signals were recorded and filtered through a bandpass filter (0.3–3 kHz). The nearby four channels of the probe were grouped as tetrodes, and semiautomatic spike sorting was performed by using Offline Sorter (Plexon). Semiautomated clustering was carried out based on the first three principal components of the spike waveform on each tetrode channel using a t-distribution EM scan algorithm (scanned over a range of 10–30 degrees of freedom) and then evaluated with sort quality metrics. Clusters with isolation distance <20 and L-ratio >0.1 were discarded. Spike clusters were classified as single units only if the waveform signal-to-noise ratio exceeded 4 (12 dB) and the interspike intervals exceeded 1.2 ms for >99.5% of the spikes.

**Optrode recording.** *Vglut2*-positive neurons were genetically tagged by crossing *Vglut2*-Cre mice with Ai27 mice (Cre-dependent ChR2 reporter line). The optrode (A1x16-Poly2-5mm-50s-177-OA16LP, 16 contacts separated by 50  $\mu$ m, the distance between the tip of the optic fiber and the probes was 200  $\mu$ m, 0.22 NA, NeuroNexus Technologies) was connected to an LED light source (480 nm, Thorlabs) with an optic fiber. To identify ChR2<sup>+</sup> neurons, LED pulse trains of 5 or 10 Hz (5-ms pulse duration, total duration of 100 ms, controlled with an Arduino microcontroller) were delivered intermittently, after we finished recording spontaneous activity. To assess whether these units were driven directly by ChR2 or indirectly by synaptic connections, the onset latency relative to each light pulse was analyzed. Only spikes with latency <4 ms were considered to be directly stimulated in this study. The waveform similarity between LED-evoked and spontaneously generated spikes was analyzed, and correlation coefficient >0.9 was used as a criterion for determination of the same unit.

**Image acquisition.** To check the expression of eYFP, GFP or mCherry or electrode tracks (coated with Dil), animals were deeply anesthetized using urethane (25%) and transcardially perfused with PBS and paraformaldehyde (4% in PBS). Coronal brain sections (150  $\mu$ m) were made with a vibratome (Leica Microsystems) and stained with Nissl reagent (Deep Red, Invitrogen) for 2 h at room temperature. Each slice was imaged under a confocal microscope (Olympus).

**Behavioral tests.** All behavioral tests were conducted in a sound attenuation booth during the dark cycle of the mice with dim ambient light. To test for potential sex dimorphism, equal numbers of animals of each sex were used. Because no difference in mPOA-induced anxiety was observed between males and females, only male animals were used for later inactivation experiments and manipulations of downstream targets. A 72-h gap was applied if the same animal was tested in multiple behavioral sessions.

**Aversive stimulation application.** Animals were exposed to cold water (15 °C), a heat plate (50 °C) or electrical foot shocks (0.3 mA, 0.5 Hz, 20-ms pulse duration) for 5 min. Anxiety-related behavior tests were performed 1 h after treatment.

**Open-field test.** A white behavior test box (60 cm × 60 cm × 30 cm, length × width × height) was virtually divided into a center field (center, 30 × 30 cm) and a periphery field. For each test, the mouse was placed in the periphery, and the locomotion of the animal was recorded with a video camera for 20 min to measure the time spent in the center or peripheral area.

**Elevated plus maze test.** A crossed maze with two closed and two open arms was elevated 30 cm above the ground. The mouse was placed in the center of

the crossed maze, and the locomotion of the animal was recorded with a video camera for 5 min.

**Real-time place preference test.** A clear acrylic behavior box (40 cm × 20 cm × 20 cm, divided into two chambers, placed in a larger white foam box) with normal bedding materials was used. For each trial, the mouse was initially placed in the non-stimulation chamber, and LED (480 nm, 10 Hz, 5-ms pulse duration) stimulation was constantly delivered once the animal entered the stimulation chamber and was stopped when the animal exited the chamber. The total duration of each test session was 20 min. Animals were returned to their home cage after each test session. The stimulation chamber was randomly assigned to each animal and balanced for the whole group. Behavioral data was recorded with a web camera. LED stimulation was automatically close-loop controlled by customized software (written by G.-W.Z. in Python 3.4) that detects the location of the animal in real-time. The online analysis was performed as described below.

**Conditioned place preference test.** A clear acrylic behavior box (40 cm × 20 cm × 20 cm, placed in a larger foam box) was divided into three chambers. The middle chamber has a gray smooth metal plate floor, the left chamber has white walls and a grid-wire floor, and the right chamber has black walls and a parallel-wire floor. On day 1, each animal was placed in the middle chamber, and no preference toward either the left or right chamber was observed. The black or white chamber was then assigned randomly as the stimulation chamber for that animal. On the 2nd and 3rd days, the animal was confined in the stimulation chamber for 20 min while LED stimulation was applied. Four hours later, the animal was also placed in the other chamber with no treatment for 20 min. On day 4, the animal was placed in the middle chamber and could freely access all chambers.

**Shelter time test.** A clear acrylic behavior box (20 cm × 20 cm × 20 cm) novel to the animal to be tested was used. A triangular shelter was placed at the corner. The animal was placed in the chamber, and locomotion was recorded with a camera. The percentage of time spent in the shelter and outside the shelter was analyzed offline using the object detection software described below.

**Dark-light box test.** An acrylic behavior box (40 cm × 20 cm × 20 cm) was divided into a dark chamber (10 cm × 20 cm × 20 cm) and a light chamber (30 cm × 20 cm × 20 cm). The dark chamber was shielded with black aluminum foil. The animal was placed in the light side at the beginning, and its behavior was recorded with a camera. The time spent on the light side was analyzed using the object detection software described below.

**Pup-directed aggression test.** Virgin male mice were housed individually for 5 d before behavioral tests. The test was conducted in the home cage of the virgin male. After habituation for 30 min, one C57BL/6 pup (<4 d old) was introduced to the far-side corner relative to the nest in the home cage. A trial was defined as an attack trial if the virgin male bit the pup within 15 min. Grooming was defined as sniffing and licking of the pup. LED stimulation was applied once the male started exploring the pup. Each trial was terminated once the male bit the pup, and the pup was immediately killed. The LED-on and LED-off trials were randomly assigned across different testing days, with a resting time of 72 h in between. Each animal was tested for 1–3 trials, and only one trial was performed on a testing day.

**Pup-induced anxiety test.** A foreign C57BL/6 pup (<4 d old) was introduced to the home cage of the virgin male. The pup was protected by using a transparent box with holes that would not block the pup odor or sound. The exposure lasted for 15 min, and the virgin male was subjected to the OFT and the EPM test immediately after the exposure.

**Intermale aggression test.** Virgin male mice were housed individually before the intermale aggression test, which was conducted in the home cage of the virgin male (resident cage). The virgin male was briefly exposed to a female mouse for 1 h, 2 d before the test. After habituation for 30 min, a castrated younger male (4 weeks old) with wild-type male fresh urine odor was introduced to the resident cage. A trial was defined as a fighting trial if the resident virgin male bit the intruder mouse. LED-on and LED-off trials were randomized across different testing days, with a resting time of 72 h in between.

**Three-dimensional object dislocation test.** The animal to be tested was habituated to a clear acrylic behavior box (20 cm × 20 cm × 20 cm) for 15 min before the test. A three-dimensional novel object (2 cm × 2 cm × 2 cm) was placed in the center of the chamber. After 3 min in the LED-off block, LED stimulation was applied for 3 min (10 Hz), followed by a 3 min in the LED-off block. The traveling distance of the three-dimensional object was calculated offline using customized software (written by G.-W.Z. in Python 3.4).

**Food intake test.** Mice were housed with ad libitum access to food and water. Just before the behavioral test, the animal was deprived of food for 24 h with ad libitum access to water. During a 2-h test block, the animal gained access to food, and LED

stimulation (10 Hz, 5-ms duration) was continuously applied. The weight of food consumed was measured after the test block. For chemogenetic manipulation, the test was started 20 min after the CNO injection (intraperitoneal).

**Thermoregulation test.** Core body temperature (anal temperature) was measured after optogenetically stimulating with light for 30 min (10 Hz, 5-ms pulse duration).

**Real-time animal detection and closed-loop optogenetic control.** Customized mouse detection software was used for online real-time animal detection (written by G.-W.Z. in Python 3.4, <https://www.python.org>, with OpenCV library, <https://opencv.org>)<sup>27,52</sup>. The behavior of the animal was monitored using an infrared camera at 24 fps. Next, each frame was Gaussian blurred and then binarized. The gravity center for the detected contour was used to determine the location of each animal. In the two-chamber PPT, the stimulation chamber was randomly assigned (balanced within the group) to each animal. Once the mouse entered the stimulation chamber, a computer-controlled Arduino microcontroller (<https://www.arduino.cc/>) would generate TTL signals to drive the LED light source (Thorlabs). The behavior test was run automatically without experimenter interference, and the result was calculated immediately after each experiment.

**Pupil size measurement and offline quantification.** Animals were head fixed. A CMOS camera (Point Grey, FL3-U3-13Y3M-C, equipped with a Fujinon 1:1.4/9mm lens, HF9HA-1B) was used to capture images of the right eye. Ambient light was provided using a 13-inch monitor (Dell) at an illuminance of ~58 lx. An infrared LED array was used to provide infrared illumination. Image acquisition (25 fps) was synchronized with the optogenetic LED stimulation using a computer with a data acquisition card (National Instruments) and customized software (written by L.S. in LabVIEW). The pupil size was analyzed offline (software written by G.-W.Z. in Python 3.4): each frame was Gaussian filtered, and the black pupil was extracted using a threshold adjusted for each experiment. The nearest eclipse was fitted to estimate the diameter of the pupil. For each experiment, a few frames were dropped due to eye blinking, and the corresponding pupil size value was estimated using interpolation based on five frames before and after the eye blink.

**Histology.** Animals were killed 3 h after exposure to water (15 °C), a heat plate (50 °C) or electrical foot shock (0.3 mA, 0.5 Hz, 20-ms pulse duration). For control experiments, animals were subjected to the same handling at room temperature, without shock or water (Extended Data Fig. 1a,b). The brain was fixed overnight and sectioned at a thickness of 50 μm. Immunohistochemistry was performed according to standard protocol with goat anti-c-Fos antibody (1:1,000, Santa Cruz Biotechnology). For colabeling of Vglut2 and c-Fos expression, Vglut2-Cre-Ai14 transgenic animals were used.

**Slice recording.** To confirm the connectivity between mPOA glutamatergic axons and PAG neurons, *Vglut2*-ires-Cre mice were injected with AAV2/1-pEF1α-DIO-hChR2-eYFP into the mPOA and used for slice recording. Three weeks following injections, animals were decapitated following urethane anesthesia, and the brain was rapidly removed and immersed in an ice-cold dissection buffer (composition, 60 mM NaCl, 3 mM KCl, 1.25 mM NaH<sub>2</sub>PO<sub>4</sub>, 25 mM NaHCO<sub>3</sub>, 115 mM sucrose, 10 mM glucose, 7 mM MgCl<sub>2</sub>, 0.5 mM CaCl<sub>2</sub>, saturated with 95% O<sub>2</sub> and 5% CO<sub>2</sub>; pH 7.4). Coronal slices at a thickness of 350 μm were sectioned with a vibrating microtome (Leica, VT1000s) and recovered for 30 min in a submersion chamber filled with warmed (35 °C) ACSF (composition, 119 mM NaCl, 26.2 mM NaHCO<sub>3</sub>, 11 mM glucose, 2.5 mM KCl, 2 mM CaCl<sub>2</sub>, 2 mM MgCl<sub>2</sub>, 1.2 mM NaH<sub>2</sub>PO<sub>4</sub>, 2 mM sodium pyruvate, 0.5 mM VC). PAG neurons surrounded by eYFP<sup>+</sup> fibers were visualized under a fluorescence microscope (Olympus, BX51 WI). Patch pipettes (resistance of ~4–5 MΩ) filled with a cesium-based internal solution (composition, 125 mM cesium gluconate, 5 mM TEA-Cl, 2 mM NaCl, 2 mM CsCl, 10 mM HEPES, 10 mM EGTA, 4 mM ATP, 0.3 mM GTP and 10 mM phosphocreatine, pH 7.25; 290 mOsm) were used for whole-cell recordings. Signals were recorded with an Axopatch 700B amplifier (Molecular Devices) under voltage-clamp mode at a holding voltage of -70 mV for excitatory currents, filtered at 2 kHz and sampled at 10 kHz. Tetrodotoxin (1 μM) and 4-aminopyridine (1 mM) were added to the external solution for recording monosynaptic responses to blue light stimulation (5-ms pulse, power of 3 mW, 10–30 trials). CNQX (20 μM, Sigma-Aldrich) was added to the external solution to block glutamatergic currents.

For testing the efficacies of ChR2, ArchT, hM4D(Gi) and hM3D(Gq), brain slices were prepared similarly, and whole-cell current-clamp recordings were made from neurons expressing ChR2, ArchT, hM4D(Gi) or hM3D(Gq). A train of blue light pulses at different frequencies (1–20 Hz, 5-ms pulse duration) was applied to measure spike responses of ChR2-expressing neurons. Green light stimulation (10-s duration) was applied to measure hyperpolarization in ArchT-expressing neurons. For neurons expressing hM4D(Gi) or hM3D(Gq), spontaneous spikes were recorded before and after perfusion with CNO (10 μM) and after washing out CNO.

**Cell-type specific monosynaptic retrograde tracing.** To trace the monosynaptic input to Vglut2<sup>+</sup> neurons in the mPOA, AAV1-DIO-FLPo-WPRE-hGHPA,

AAV8-CAG-fDIO-TVA-mCherry and AAV<sub>D1</sub>-CAG-fDIO-oG-WPRE were mixed (1:1; 80 nl) and stereotactically injected into the mPOA of *Vglut2*-Cre mice. After 2 weeks, *EnvA-EnvG*-deleted rabies-GFP was injected into the mPOA. The animal was killed 1 week later. Brain tissue was fixed, sectioned and imaged using a confocal microscope.

**Statistics.** When it was possible, a prior power analysis was used to determine sample sizes. Otherwise, sample sizes were selected based on previous experience from related research or literature. Animals were randomly assigned to control and treatment groups. For animals with multiple treatments, the sequence of treatments was randomized. Investigators were not blinded to group allocation or data collection, but the analyses of behavioral data were performed blind to the conditions of experiments, as data obtained under different conditions were pooled together for an automatic batch analysis with computer software. Prism version 8 software (GraphPad) and R were used for statistical analysis. The Kolmogorov-Smirnov test was used to test for normality. The Mann-Whitney test was used for non-normal data. The Kolmogorov-Smirnov test was used to compare the response difference between shock-exposed and control groups. One-way ANOVA and two-way ANOVA and post hoc Tukey's multiple comparisons were used to test significance between samples. For two-group comparison of normal data, significance was determined by *t*-test. Paired *t*-tests were used to compare data from the same animal. In this study, no data were excluded from analysis.

**Reporting Summary.** Further information on research design is available in the Nature Research Reporting Summary linked to this article.

## Data availability

All data that support the findings of this study are available from the corresponding authors upon request.

## Code availability

The Python code for animal detection is available at <https://github.com/GuangWei-Zhang/TraCon-Toolbox>. The custom pupil size detection Python code and custom MATLAB code for fiber photometry or electrophysiological data analysis will be provided upon request to the corresponding authors.

## References

51. Tervo, D. G. R. et al. A designer AAV variant permits efficient retrograde access to projection neurons. *Neuron* **92**, 372–382 (2016).
52. Zhang, G., Shen, L., Li, Z., Tao, H. W. & Zhang, L. I. Track-Control, an automatic video-based real-time closed-loop behavioral control toolbox. Preprint at *bioRxiv* <https://doi.org/10.1101/2019.12.11.873372> (2019).

## Acknowledgements

This work was supported by grants from the US National Institutes of Health to H.W.T. (EY019049, MH116990) and L.I.Z. (R01DC008983, RF1MH114112, MH116990). We thank Y. Xiong and J. Wei at Southern Medical University for generous help with behavioral experiments.

## Author contributions

G.-W.Z. performed behavioral and photometry experiments and data analysis. L.S. performed optrode recording experiments. A.-H.J. contributed to immunohistochemistry experiments and image analysis. C.T. and B.P. performed slice recording experiments. Z.L. helped with photometry experiments. L.I.Z. and H.W.T supervised the project. H.W.T., G.-W.Z. and L.I.Z. wrote the manuscript.

## Competing interests

The authors declare no competing interests.

## Additional information

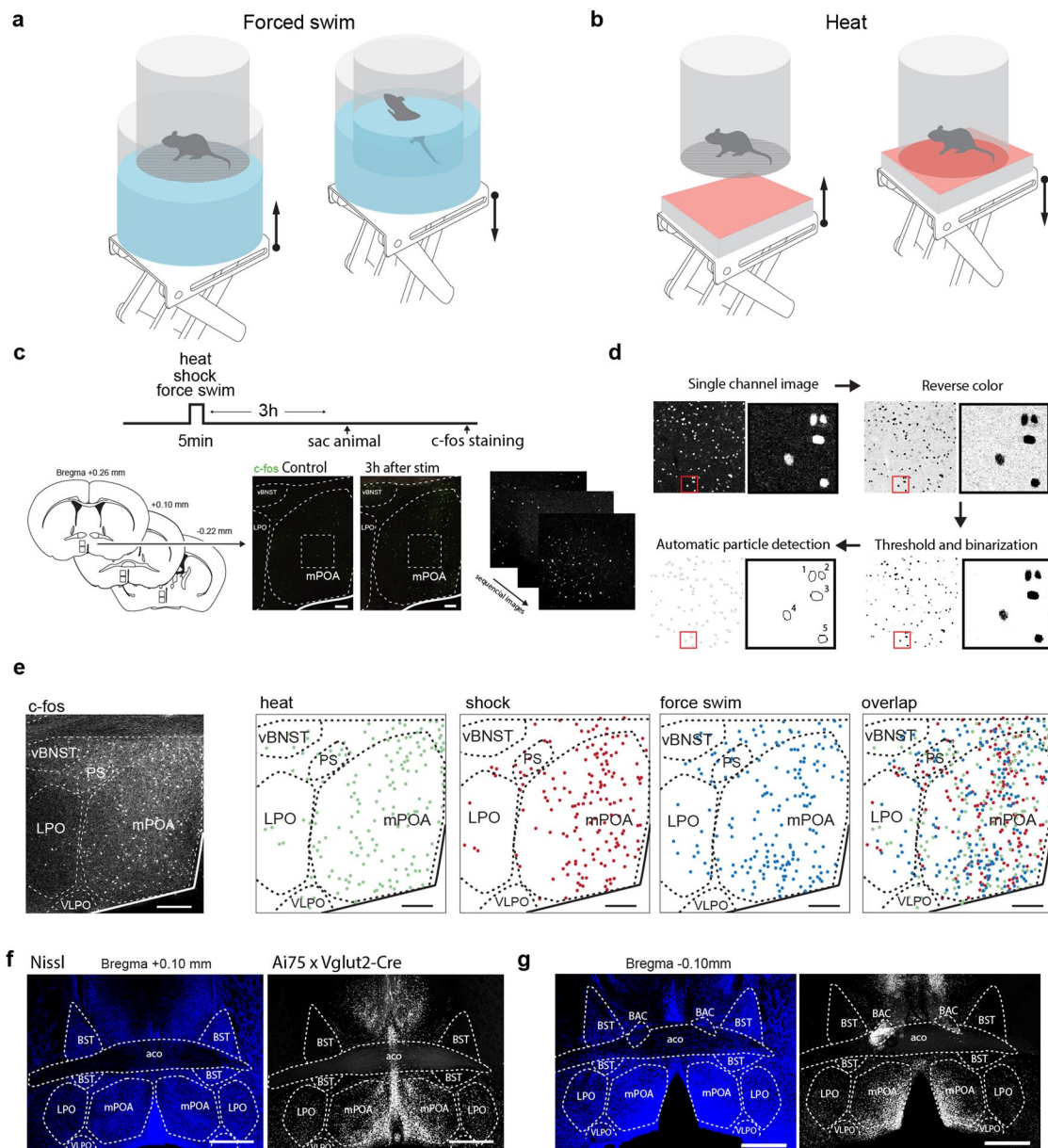
**Extended data** is available for this paper at <https://doi.org/10.1038/s41593-020-00784-3>.

**Supplementary information** The online version contains supplementary material available at <https://doi.org/10.1038/s41593-020-00784-3>.

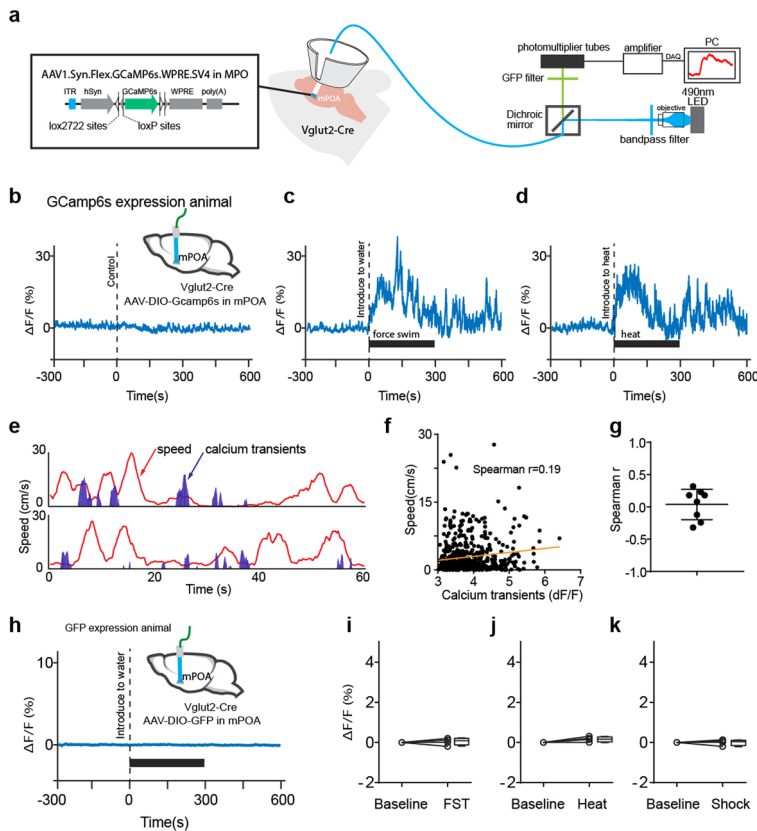
**Correspondence and requests for materials** should be addressed to L.I.Z. or H.W.T.

**Peer review information** *Nature Neuroscience* thanks the anonymous reviewers for their contribution to the peer review of this work.

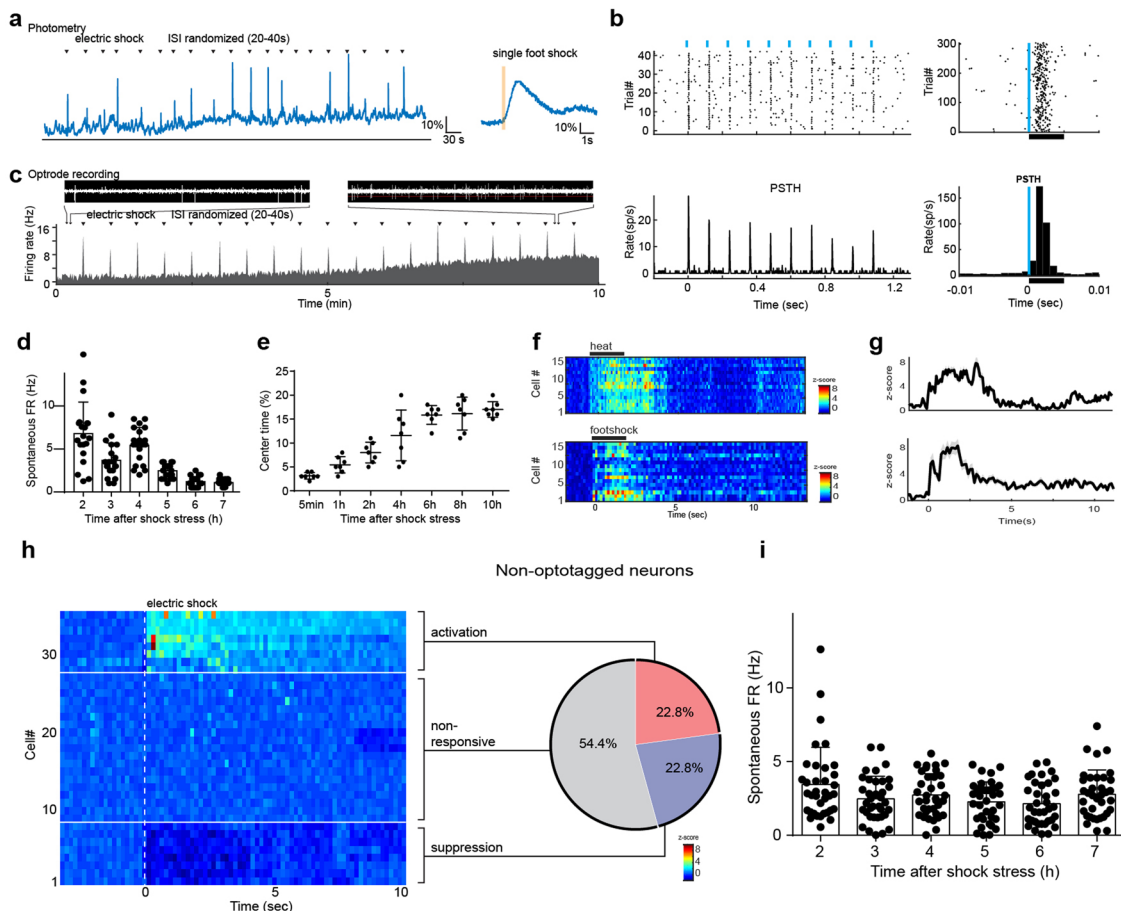
**Reprints and permissions information** is available at [www.nature.com/reprints](http://www.nature.com/reprints).



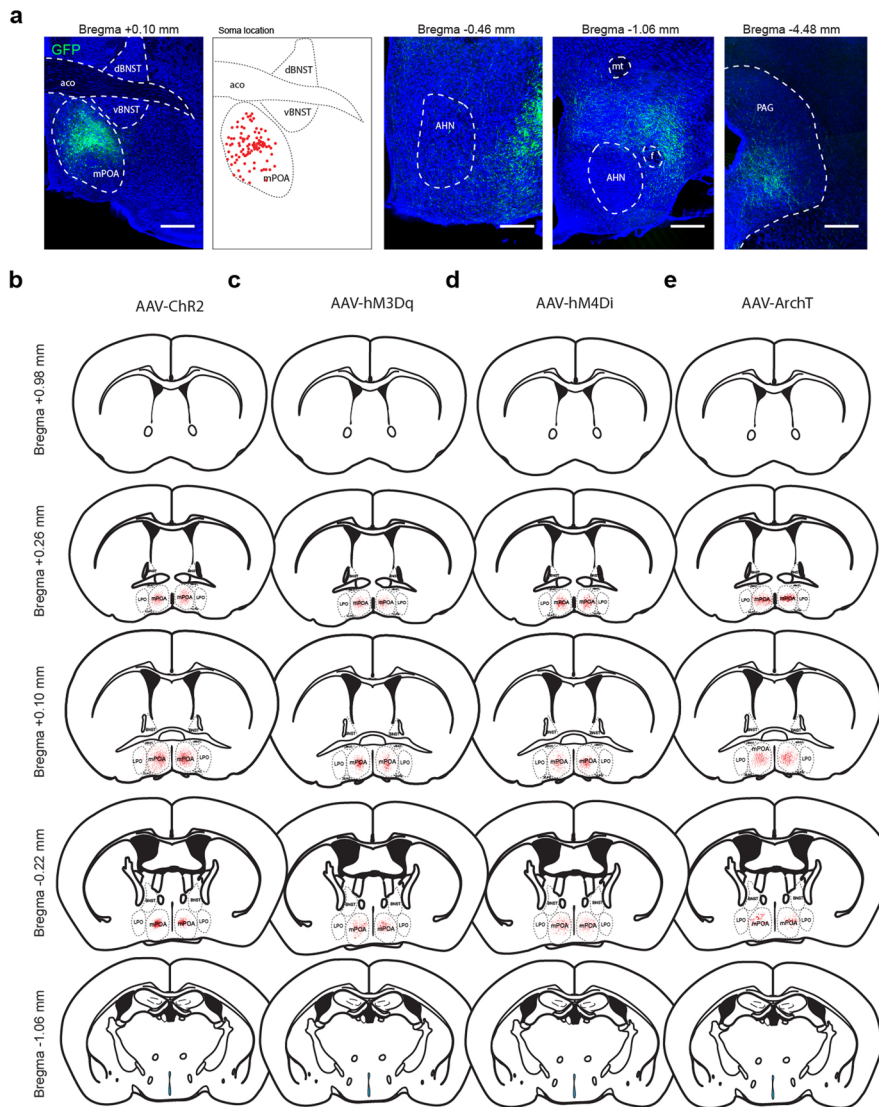
**Extended Data Fig. 1 | Quantification pipeline for c-fos staining and Vglut2 expression in mPOA. (Associated with Fig. 1.)** **a**, Illustration of force swimming application. The bottom of the test chamber was a metal mesh. For the control experiment, the animal was placed in the same context without being submerged into water (condition on the left). **b**, Illustration of heat plate application. For the control experiment, the animal was placed in the same context without being touched by the heat plate (condition on the left). **c**, Protocol for c-fos staining and imaging. Animals were exposed to one of the stressors for 5 min and were sacrificed 3 hours after the treatment. Scale, 100  $\mu$ m. **d**, Pipeline for image processing and cell counting. **e**, Spatial distribution of c-fos+ cells under treatments of three different stressors. LPO, lateral preoptic area; VLPO, ventral lateral preoptic area. Scale, 200  $\mu$ m. **f**, Left, Nissl staining; right, tdTomato expression in the same coronal brain section. Images were obtained from transgenic mice by crossing Ai75 (Cre-dependent nucleus-targeted tdTomato reporter) and Vglut2-Cre. **g**, A more posterior section. BAC, bed nucleus of the anterior commissure; aco, anterior commissure. Scale, 500  $\mu$ m. Images in **c,d** are representative of  $n=9$  animals, Images in **e,f,g** are representative of  $n=3$  animals.



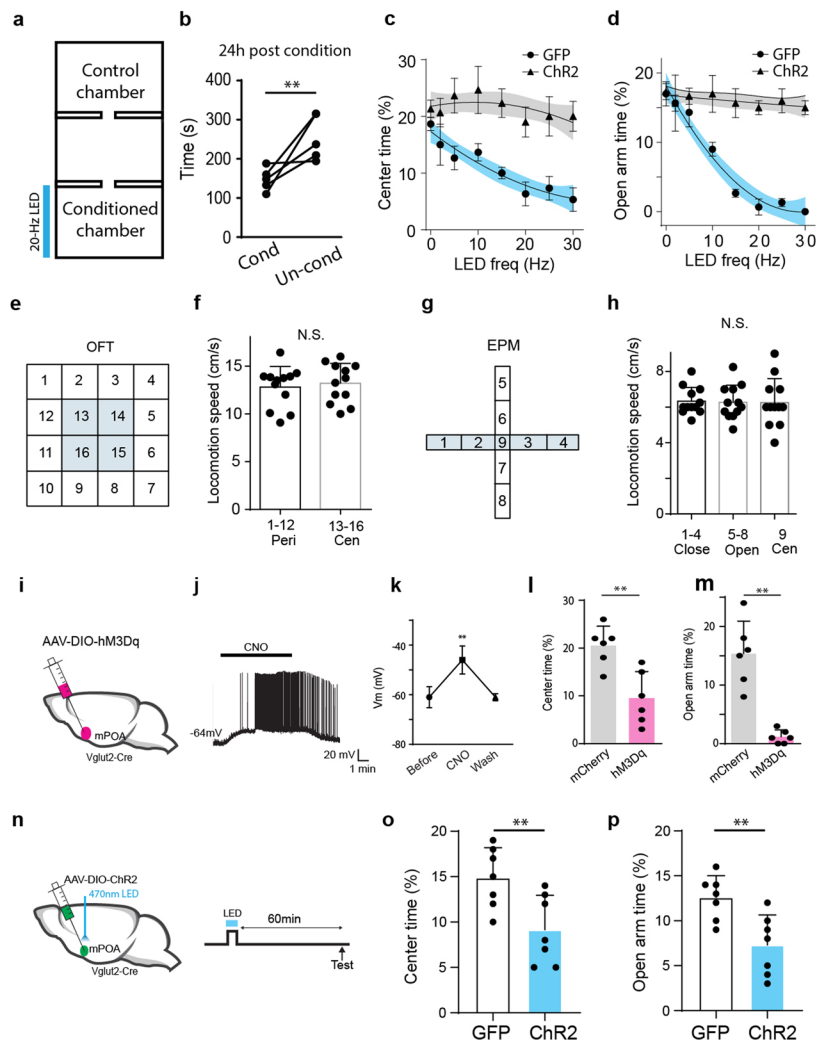
**Extended Data Fig. 2 | Quality control for fiber photometry. (Associated with Fig. 1).** **a**, Illustration of the fiber photometry setup. A protective cover helps to prevent the optic fiber from bumping against the wall of the test box/chamber. Neurons express Cre-dependent GCaMP6s. **b**, Example full trace of calcium signals in the control condition for forced swimming. Dashed line indicates the presumptive operation time (no operation was actually applied). **c**, Example full trace of calcium signals for forced swimming application. Bar represents the exposure duration. **d**, Example full trace of calcium signals for heat plate application. **e**, Plot of calcium transients (blue) and concurrent locomotion speed (red, freely moving) in an open field. Z-score = 3 was used as the detection threshold. **f**, Plot of locomotion speed vs. amplitude of calcium transients. **g**, Spearman  $r$  calculated for each mouse. N = 8 animals. Bars represent mean  $\pm$  s.d. **h**, Fluorescence signals in a control animal expressing GFP only. Black bar marks duration of forced swimming exposure. **i**, Peak calcium transients during the baseline period and stressor application for GFP control animals ( $n=4$ ). Statistics can be found in Fig. 1. FST, forced swimming test. **j**, Heat plate exposure in GFP control animals ( $n=4$ ). **k**, Electric shock exposure in GFP control animals ( $n=4$ ). (see Supplementary Table 1 for detailed statistics).



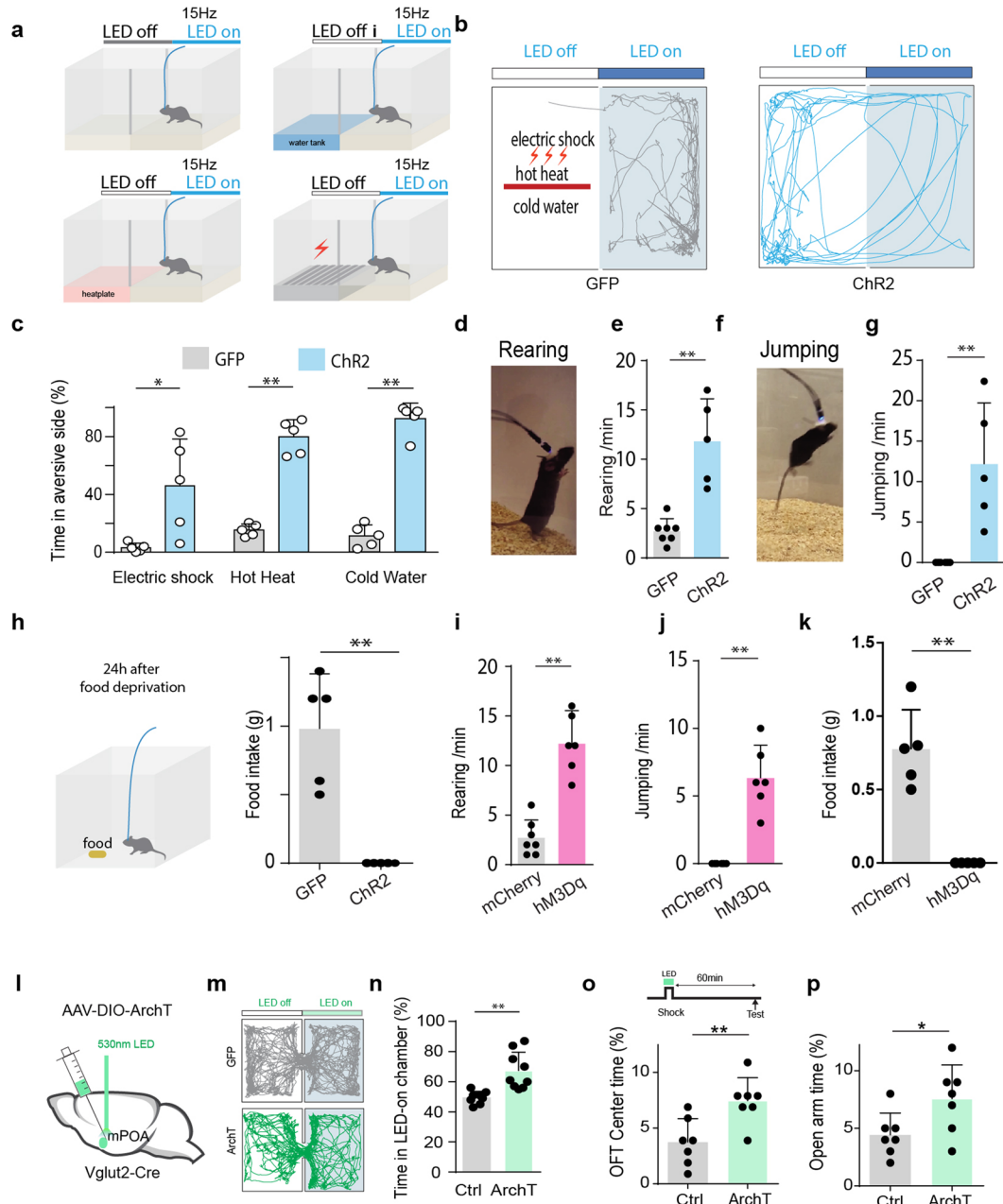
**Extended Data Fig. 3 | Optrode recording. (Associated with Fig. 1).** **a**, Top, example full trace of fiber photometry recording (left, each black dot represents one application of foot shocks) and average  $\text{Ca}^{2+}$  response (averaged over trials) to a foot shock application (right). **b**, Top, raster plot of LED-induced spike responses for an example mPOA glutamatergic neuron. Blue dots indicate the duration of LED pulse (5ms). Bottom, corresponding peri-stimulus spike time histogram (PSTH). Raster plot and PSTH for spikes induced by a single LED pulse (blue line). Thick black line indicates the duration of LED stimulation. Only cells show 1<sup>st</sup> spike latency shorter than 4ms were considered as valid optogenetically-identified Vglut2+ neurons and included for analysis. **c**, Example full trace of single-unit responses to repeated foot shock stimulation. Spontaneous spikes before the first and last electric shock application are shown on top for visualization. **d**, Spontaneous firing rates of mPOA opto-IDed Vglut2+ neurons at different time points after exposure to foot shocks. N=19 cells from 2 animals. **e**, Center time in OFT performed at different time points after exposure to foot shocks. N=7 animals. **f**, Heatmaps of single-cell spike responses to heat (top) and electric shocks (bottom) of opto-IDed Vglut2+ neurons. The same cells are shown to demonstrate multimodal responses. **g**, Population average of PSTHs from cells shown in **(f)**. **h**, Heatmap of single-cell spike responses to electric shocks for non-optotagged (presumably Vglut2-) neurons. Pie chart shows the percentage of presumably Vglut2- neurons that shows activated, no, or suppressive responses to electric shocks, respectively. Spontaneous firing rates of non-optotagged neurons at different time points after exposure to foot shocks. N=35 cells from 2 animals.



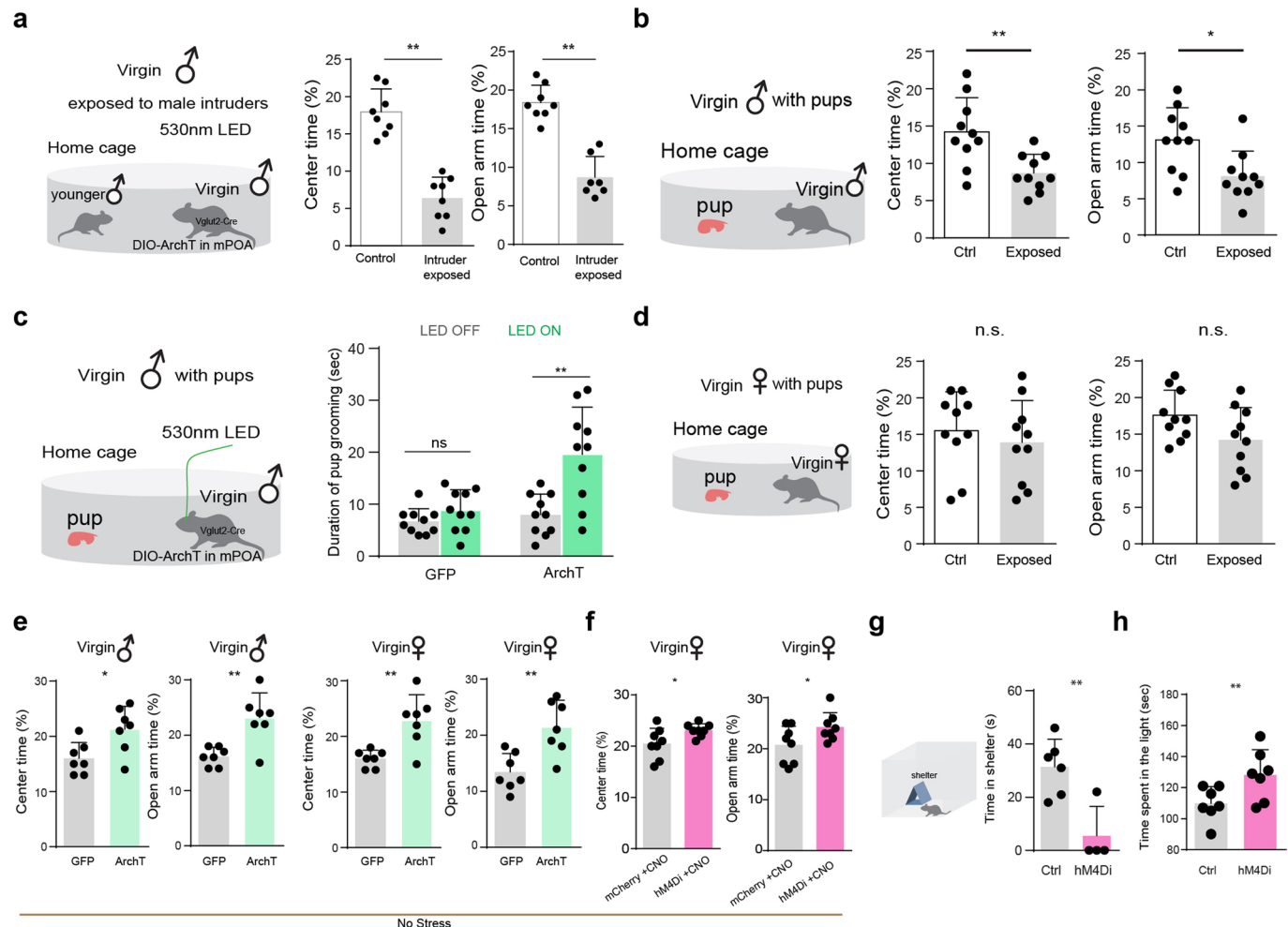
**Extended Data Fig. 4 | Locations of somas with viral expression. (Associated with Figs. 2–4).** Schematic coronal sections ranging from 0.98 mm anterior to 1.06 mm posterior to Bregma. **a**, Left two, Cre-dependent GFP expression at the injection site in a Vglut2-Cre mouse and spatial distribution of expressing cell bodies. Right three, axons in more posterior sections. Same image as in Fig. 5a. Blue, Nissl staining. Scale, 300  $\mu$ m. **(b)** **a**, Representative images of GFP-labeled mPOA glutamatergic neurons (left) and their axons in PAG (right). Scale bar: 500  $\mu$ m. **c**, Superimposed ChR2-EYFP expressing cell locations for all mice from anterior to posterior sections. Each small red dot represents one cell. **d**, Superimposed hM3Dq-mCherry expressing cell locations for all mice. **e**, Superimposed hM4Di-mCherry expressing cell locations for all mice. **f**, Superimposed ArchT-GFP expressing cell locations for all mice. Images in a are representative of n=6 animals.



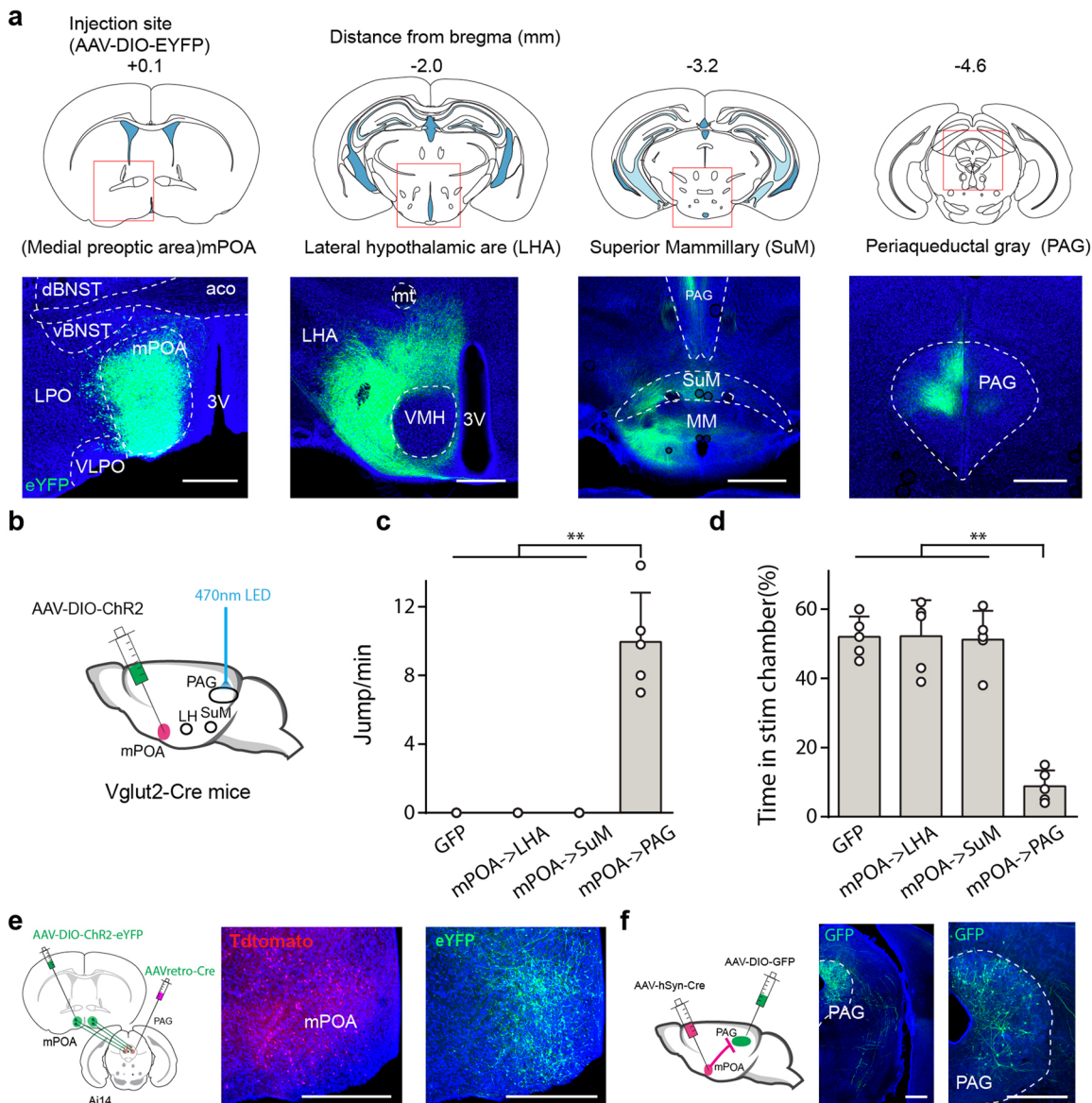
**Extended Data Fig. 5 | Activation of mPOA Vglut2 neurons. (Associated with Fig. 2).** **a**, Experimental setup for conditioned place preference test. During conditioning, the animal was subjected to LED stimulation whenever it was in the conditioned chamber. **b**, Conditioned place aversion tested 24 hours after pairing photo-stimulation with one chamber. Time spent in the conditioned chamber (Cond) or unconditioned chamber (Un-cond) was quantified. \*\*P < 0.01, Mann-Whitney test, n = 5 animals. **c**, Quantification of center time in OFT under different light stimulation frequencies (Kolmogorov-Smirnov test with Bonferroni correction, P < 0.001, n = 5 and 5 animals for GFP control and ChR2 groups respectively). Each animal was tested for one session per day with stimulation frequencies randomly selected. **d**, Quantification of open-arm time in EPM (Kolmogorov-Smirnov test with Bonferroni correction, P < 0.001, n = 5 and 5 animals for GFP control and ChR2 groups respectively). **e**, The OFT arena was divided into 16 subregions and locomotion speed were calculated for each specific subregion. **f**, Locomotion speed in center vs peripheral subregions. Each dot is one animal. N.S., non-significant; paired t test. N = 12. **g**, The EPM arena was divided into 9 subregions. **h**, Locomotion speed in closed-arm, open-arm and center subregions. N = 12. **i**, Expressing hM3Dq receptors in mPOA glutamatergic neurons. **j**, Raw recorded trace of the membrane potential of a hM3Dq-expressing mPOA glutamatergic neuron in response to CNO application in slice recording. **k**, Subthreshold membrane potential voltages before and after perfusion of CNO as well as after washing out CNO. \*\*P < 0.01, one-way repeated-measures ANOVA, n = 5 cells from 2 animals. **l**, Quantification of center time in OFT for mCherry control and hM3Dq expressing animals. \*\*P < 0.01, Mann-Whitney test, n = 6 animals for each group. **m**, Quantification of open-arm time in EPM for mCherry control and hM3Dq expressing animals. \*\*P < 0.01, Mann-Whitney test, n = 6 animals for each group. **n**, Experimental timeline: expressing ChR2 in mPOA glutamatergic neurons, optogenetic stimulation for 5-min (20 Hz) and anxiety-related behavioral test one hour later. **o**, Quantification of center time in OFT for GFP control and ChR2-expressing groups. \*\*P < 0.01, Mann-Whitney test, n = 7 animals for each group. Quantification of open arm time in EPM for GFP control and ChR2-expressing groups. \*\*P < 0.01, Mann-Whitney test, n = 7 animals for each group. (see Supplementary Table 1 for detailed statistics).



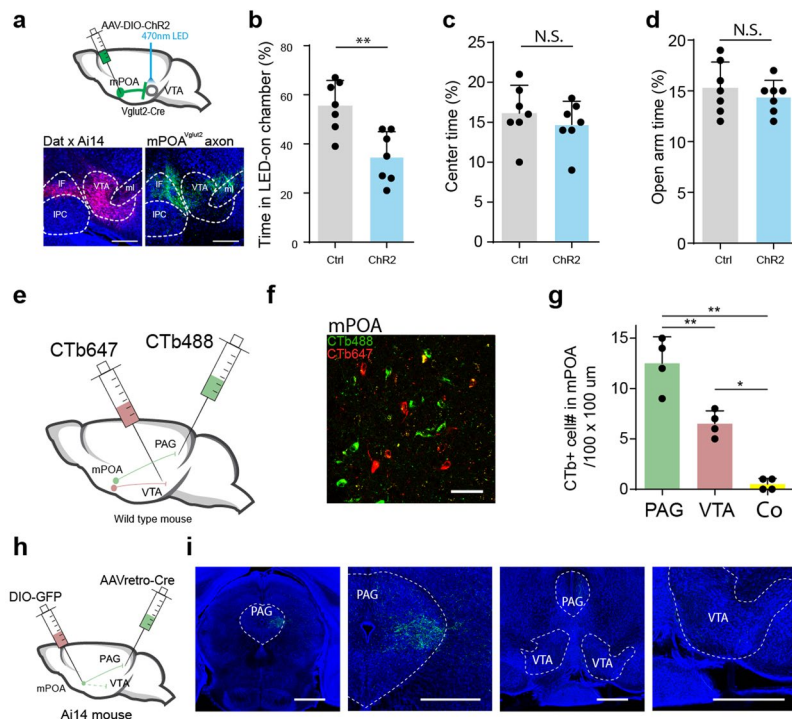
**Extended Data Fig. 6 | Strong activation of mPOA glutamatergic neurons. (Associated with Fig. 2).** **a**, Illustration of conflict tests. **b**, Movement tracing of a GFP control animal (left) and a ChR2-expressing animal (right) in a conflict test. Photostimulation at 15 Hz was applied whenever the mouse was in the light gray marked zone. **c**, Percentage time spent in the physically harmful side for control and ChR2 animals. \*P < 0.05; \*\*P < 0.01, Mann-Whitney test, n=6 animals for each group. **d**, Photo of mouse rearing during LED activation of mPOA glutamatergic neurons at 15 Hz. **e**, Frequency of rearing in GFP control (n=7) and ChR2 expressing (n=5) animals. \*\*P < 0.01, Mann-Whitney test with Bonferroni correction. **f**, Photo of mouse jumping during LED activation of mPOA glutamatergic neurons at 15 Hz. **g**, Frequency of jumping in GFP control (n=7) and ChR2-expressing (n=5) animals. \*\*P < 0.01, Mann-Whitney test with Bonferroni correction. **h**, Food intake within 2 hours after being food-deprived for 24 hours. During the 2h test, mPOA glutamatergic neurons were photo-stimulated continuously. \*\*P < 0.01, Mann-Whitney test, n=5 animals for each group. **i**, Frequency of rearing in mCherry control (n=7) and hM3Dq-expressing (n=6) animals. \*\*P < 0.01, Mann-Whitney test with Bonferroni correction. **j**, Comparison of rearing frequency between mCherry control (n=7) and hM3Dq-expressing (n=6) animals. \*\*P < 0.01, Mann-Whitney test with Bonferroni correction. **k**, Food intake within 2 hours after being food-deprived for 24 hours. CNO injection (i.p.) was performed 20 min before the test. \*\*P < 0.01, Mann-Whitney test with Bonferroni correction, n=5 for each group. **l**, Strategy of viral injection. **m**, Movement tracing of a GFP control animal (upper) and an ArchT-expressing animal (lower) in a two-chamber place preference test. Continuous LED stimulation was applied whenever the animal stayed in the light gray marked chamber. **n**, Percentage time spent in the LED-on chamber. \*\*P < 0.01, Mann-Whitney test, n=9 (5 males) for each group. **o**, Upper, experimental time line. LED light was applied only during the electric shocks. Center time in OFT for GFP control (n=7) and ArchT-expressing (n=7; 4 males) animals. \*\*P < 0.01, Mann-Whitney test. **p**, Open-arm time in EPM for GFP control (n=7) and ArchT-expressing (n=7; 4 males) animals. \*\*P < 0.05, Mann-Whitney test, n=7 animals for each group. (see Supplementary Table 1 for detailed statistics).



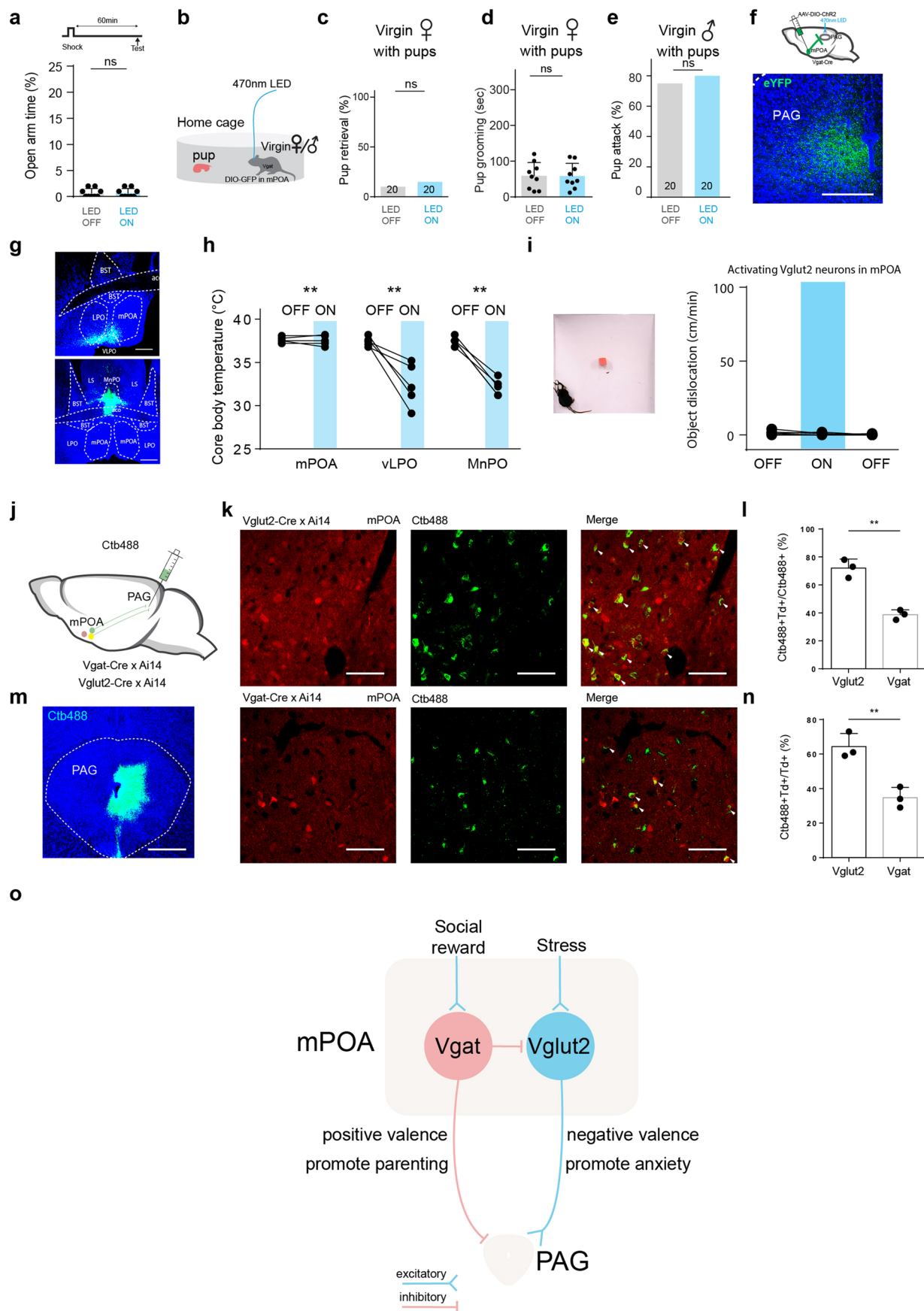
**Extended Data Fig. 7 | Anxiety tests after exposure to social stress. (Associated with Fig. 4).** **a**, Anxiety-like behaviors of virgin males with or without exposure to male intruders. \*\*P < 0.01, Mann–Whitney test, n=8 animals for each group. **b**, Anxiety-like behaviors for virgin males with or without exposure to foreign pups. \*\*P < 0.01, Mann–Whitney test, n=10 animals for each group. **c**, Duration of pup grooming for virgin males in LED-off and LED-on conditions. \*\*P < 0.01, Mann–Whitney test with Bonferroni correction, n=10 animals for each group. **d**, Anxiety-like behaviors of virgin females with or without exposure to foreign pups. ‘n.s.’, not significant, Mann–Whitney test, n=10 animals for each group. **e**, Anxiety-related tests in virgin males/females not exposed to stress with (green) and without (grey) optogenetic silencing of mPOA Vglut2 neurons. \*P < 0.05, \*\*P < 0.01, Mann–Whitney test with Bonferroni correction, n=7 animals for each group. **f**, Anxiety-related tests in virgin females not exposed to stress with (green) and without (grey) chemogenetic silencing of mPOA Vglut2 neurons. \*\*P < 0.01, Mann–Whitney test with Bonferroni correction, n=8 animals for each group. **g**, Left, schematic open field test with a shelter. Right, total time spent in shelter within a 5-min test session. \*\*P < 0.01, Mann–Whitney test, n=6 (3 males) animals. **h**, Total time spent in the light side of a light-dark box. \*\*P < 0.01, Mann–Whitney test, n=7 (4 males) animals for each group. (see Supplementary Table 1 for detailed statistics).



**Extended Data Fig. 8 | Potential targets of mPOA glutamatergic neurons. (Associated with Fig. 5). a, Imaging area (top) and a confocal image (bottom) showing EYFP labeling in mPOA (left) and different downstream structures. Scale, 500 μm. VMH, ventral medial hypothalamic nucleus; MM, medial mammillary nucleus. b, Schematic terminal stimulation in a potential mPOA target. c, Frequency of jumping induced by activating axonal terminals of mPOA glutamatergic neurons in different target areas. \*\*P < 0.01, One-way ANOVA test, n = 5 animals for each group. GFP control group is for animals expressing GFP in mPOA with fiber implantation in mPOA. d, Two-chamber place preference test when activating axonal terminals of mPOA glutamatergic neurons in different target areas. \*\*P < 0.01, One-way ANOVA test, n = 5 animals for each group. e, Left, viral injection strategy to express ChR2 in PAG-projecting mPOA neurons in Ai14 mice. Right, images showing tdTomato- and ChR2-EYFP labeled neurons in mPOA. Scale bar, 500 μm. f, Left, viral injection strategy to transsynaptically label mPOA-recipient PAG neurons. Right, image showing labeled neurons in PAG (with a blow-up image on the right). Scale bar, 500 μm. Images in a,e are representative of n=5 animals. Images in f are representative of n =3 animals. (see Supplementary Table 1 for detailed statistics).**



**Extended Data Fig. 9 | Manipulation of the mPOA to VTA pathway. (Associated with Fig. 5).** **a**, Top, viral injection strategy. Optic cannula was implanted above VTA. Bottom, labeling of dopamine neurons (red) by crossing DAT-Cre and Ai14 mice (left) and mPOA glutamatergic axons in VTA and surrounding regions (right). Scale, 400 μm. **b**, Percentage time spent in the LED-on chamber in PPT for GFP control and ChR2-expressing animals. \*\*P<0.01, Mann-Whitney test, n = 7 (4 males) for each group. **c**, Center time in OFT. N.S., no statistical difference, Mann-Whitney test, n = 7 animals for each group. **d**, Open-arm time in EPM. Mann-Whitney test, n = 7 animals for each group. **e**, Double retrograde dye injection in PAG (green) and VTA (red). **f**, Representative image showing retrogradely labelled neurons in mPOA. **g**, Quantification of singly and doubly labeled neurons in mPOA. N=4 animals. **h**, Viral strategy to label axon collaterals of PAG-projecting mPOA neurons in VTA. **i**, Images showing many labeled axons in PAG (left two), but extremely sparse axons in VTA (right two). Injection site is shown in Fig. 5b (shared blue channel as reference). Scale, 500 μm. Images in **a,i** are representative of n = 3 animals, images in **f** are representative of n = 4 animals. (see Supplementary Table 1 for detailed statistics).



Extended Data Fig. 10 | See next page for caption.

**Extended Data Fig. 10 | Control experiments for manipulating neurons in mPOA and proposed circuit model. (Associated with Fig. 6).** **a**, Open-arm time for GFP control animals in LED-off and LED-on conditions. ‘n.s.’, non-significant, Mann–Whitney test, n=10 animals for each group. **b**, Schematic pup exposure test for virgin males or females. **c**, Percentage of trials with pup retrieval for GFP control virgin females in LED-on and LED-off conditions respectively. ‘n.s.’, non-significant, Fisher’s exact test, n=7 animals for each group. Each animal was subjected to 2–4 trials and all trials were pooled together. **d**, Duration of pup grooming for GFP control virgin females. ‘n.s.’, non-significant, Mann–Whitney test, n=9 animals for each group. **e**, Percentage of trials with pup attack for GFP control virgin males in LED-on and LED-off conditions respectively. ‘n.s.’, non-significant, Fisher’s exact test, n=7 animals for each group. Each animal was subjected to 2–4 trials and all trials were pooled together. **f**, Left, viral injection strategy and implantation of the optic fiber above PAG. Right, image showing axons of mPOA GABAergic neurons in PAG. Scale, 500 μm. **g**, Representative images showing injection sites in VLPO (top) and MnPO (bottom). Scale, 500 μm. **h**, Core body temperature measured after 10-Hz LED stimulation for 30 min in animals expressing ChR2 in mPOA, ventral lateral preoptic area (vLPO) and median preoptic area (MnPO) respectively in Vglut2-Cre animals. \*\*P < 0.01, two-tailed t-test, n=5 animals for each group. bar, s.d. **i**, Left, photo of a freely moving mouse in an open arena, with a 2x2x2cm 3D object placed in the center. The behavioral test consisted of 3 blocks: LED-off, LED-on, and then LED-off, with each lasting 3 min. 10-Hz LED stimulation was applied during the LED-on block. Right, dislocation of the 3D object by the mouse. No statistical significance was observed between blocks; two-way repeated-measures ANOVA, n=5 animals. **j**, CTb488 injection in PAG of either Vglut2-Cre::Ai14 or Vgat-Cre::Ai14 mice. **k**, Images showing overlap between CTb-labeled and Vglut2+ (top) / Vgat+ (bottom) neurons in mPOA. Scale, 200 μm. **l**, Quantification of the percentage of PAG-projecting mPOA neurons that are Vglut2+ or Vgat+. \*\*P<0.01, Mann–Whitney test with Bonferroni correction, n=3 animals for each group. Bar, s.d. **m**, Representative image showing the CTb injection site in medial PAG. **n**, Quantification of the percentage of Vglut2+ or Vgat+ mPOA neurons that were labeled by CTb injected in PAG. \*\*P<0.01, Mann–Whitney test with Bonferroni correction, n=3 animals for each group. Bar, s.d. **o**, Illustration of the proposed circuit model. Note that due to potentially different inputs, glutamatergic neurons in mPOA respond to physical and social stressors but not to social rewards, while GABAergic neurons are activated by social rewards (for example during parenting) but not stressors. Images in f are representative of n=8 animals. Images in g are representative of n=5 animals. Images in k, m are representative of n=3 animals. (see Supplementary Table 1 for detailed statistics).

## Reporting Summary

Nature Research wishes to improve the reproducibility of the work that we publish. This form provides structure for consistency and transparency in reporting. For further information on Nature Research policies, see [Authors & Referees](#) and the [Editorial Policy Checklist](#).

### Statistics

For all statistical analyses, confirm that the following items are present in the figure legend, table legend, main text, or Methods section.

n/a Confirmed

- The exact sample size ( $n$ ) for each experimental group/condition, given as a discrete number and unit of measurement
- A statement on whether measurements were taken from distinct samples or whether the same sample was measured repeatedly
- The statistical test(s) used AND whether they are one- or two-sided  
*Only common tests should be described solely by name; describe more complex techniques in the Methods section.*
- A description of all covariates tested
- A description of any assumptions or corrections, such as tests of normality and adjustment for multiple comparisons
- A full description of the statistical parameters including central tendency (e.g. means) or other basic estimates (e.g. regression coefficient) AND variation (e.g. standard deviation) or associated estimates of uncertainty (e.g. confidence intervals)
- For null hypothesis testing, the test statistic (e.g.  $F$ ,  $t$ ,  $r$ ) with confidence intervals, effect sizes, degrees of freedom and  $P$  value noted  
*Give  $P$  values as exact values whenever suitable.*
- For Bayesian analysis, information on the choice of priors and Markov chain Monte Carlo settings
- For hierarchical and complex designs, identification of the appropriate level for tests and full reporting of outcomes
- Estimates of effect sizes (e.g. Cohen's  $d$ , Pearson's  $r$ ), indicating how they were calculated

*Our web collection on [statistics for biologists](#) contains articles on many of the points above.*

### Software and code

Policy information about [availability of computer code](#)

## Data collection

We listed all softwares used in the experiments and for analysis in the Methods section. We used a custom Labview (National Instrument) program to collect the fiberphotometry signal. We used a customized Python software for real-time animal detection and trigger optogenetic stimulation. Confocal Images were captured using Fluoview1000 (Olympus). In vitro brain slice electrophysiological signals were recorded using an Axopatch 700B amplifier (Molecular Devices). In vivo electrophysiological signals were recorded using a custom Labview software.

## Data analysis

We listed all softwares used in the experiments and for analysis in the Methods section. We used customized Python code (<https://github.com/GuangWei-Zhang/TraCon-Toolbox>) to track location of animals. Customized Matlab code were used to analyze the photometry signal. In vivo electrophysiological recording data were analyzed using customized Matlab code and Python code. In vitro slice recording data were analyzed using pClamp (Molecular Devices).

For manuscripts utilizing custom algorithms or software that are central to the research but not yet described in published literature, software must be made available to editors/reviewers. We strongly encourage code deposition in a community repository (e.g. GitHub). See the Nature Research [guidelines for submitting code & software](#) for further information.

### Data

Policy information about [availability of data](#)

All manuscripts must include a [data availability statement](#). This statement should provide the following information, where applicable:

- Accession codes, unique identifiers, or web links for publicly available datasets
- A list of figures that have associated raw data
- A description of any restrictions on data availability

All data that support the findings of this study are available from the corresponding authors upon request.

# Field-specific reporting

Please select the one below that is the best fit for your research. If you are not sure, read the appropriate sections before making your selection.

- Life sciences       Behavioural & social sciences       Ecological, evolutionary & environmental sciences

For a reference copy of the document with all sections, see [nature.com/documents/nr-reporting-summary-flat.pdf](http://nature.com/documents/nr-reporting-summary-flat.pdf)

## Life sciences study design

All studies must disclose on these points even when the disclosure is negative.

Sample size	When it is possible, a prior power analysis was used to determine sample sizes. Otherwise, sample sizes were selected based on previous experience from related research and literature.
Data exclusions	No data were excluded.
Replication	Experimental findings were reliably reproduced among all subjects in all experiments comprised of multiple cohorts. In vivo recordings were conducted at least 3 cohorts of animals. Pharmacogenetic experiments were conducted with 5 cohorts of animals. Optogenetic experiments were conducted with 3 cohorts of animals. Slice recording were performed at least 2 cohorts of animals. Fiber photometry were performed at 2 cohorts of animals.
Randomization	Animals were randomly assigned to control and treatment groups. For the animals with multiple treatment, the sequence of treatment was randomized.
Blinding	Investigators were not blinded to group allocation or data collection, but the analyses of behavioral data were performed blind to the conditions of experiments as data obtained under different conditions were pooled together for an automatic batch analysis with computer softwares.

## Reporting for specific materials, systems and methods

We require information from authors about some types of materials, experimental systems and methods used in many studies. Here, indicate whether each material, system or method listed is relevant to your study. If you are not sure if a list item applies to your research, read the appropriate section before selecting a response.

Materials & experimental systems		Methods	
n/a	Involved in the study	n/a	Involved in the study
<input type="checkbox"/>	<input checked="" type="checkbox"/> Antibodies	<input type="checkbox"/>	<input type="checkbox"/> ChIP-seq
<input checked="" type="checkbox"/>	<input type="checkbox"/> Eukaryotic cell lines	<input checked="" type="checkbox"/>	<input type="checkbox"/> Flow cytometry
<input checked="" type="checkbox"/>	<input type="checkbox"/> Palaeontology	<input checked="" type="checkbox"/>	<input type="checkbox"/> MRI-based neuroimaging
<input type="checkbox"/>	<input checked="" type="checkbox"/> Animals and other organisms		
<input checked="" type="checkbox"/>	<input type="checkbox"/> Human research participants		
<input checked="" type="checkbox"/>	<input type="checkbox"/> Clinical data		

## Antibodies

Antibodies used	Primary antibodies: Goat anti-cFos (sc-52-G, Santa Cruz) Secondary antibody: Donkey anti-anti-goat Alexa 488 (A11055, Life Technologies)
-----------------	---

Validation	<a href="http://www.scbt.com/datasheet-52-c-fos-4-antibody.html">http://www.scbt.com/datasheet-52-c-fos-4-antibody.html</a>
------------	---

## Animals and other organisms

Policy information about [studies involving animals; ARRIVE guidelines](#) recommended for reporting animal research

Laboratory animals	The Vglut2-ires-Cre (Jackson stock No. 016963), Vgat-ires-Cre (Jackson stock No.016962), Ai14 (Cre-dependent tdTomato reporter line, Jackson stock No. 007914), Ai27 (Cre-dependent Chr2 reporter line, Jackson stock No.012567) and Ai75 (Cre-dependent nuclear-localized tdTomato reporter line, Jackson stock No.025106), Dat-ires-Cre (Jackson stock No.006660), C57BL/6 mice were obtained from the Jackson Laboratory. Mice were housed in a 12h light-dark cycle with ad libitum access to food and water. Experiments were performed in adult male and female mice (6-12 weeks old).
Wild animals	The study did not involve wild animals.

Field-collected samples

The study did not involve data collected from the field.

Ethics oversight

Animal experiments were conducted in accordance with the guidelines for the care and use of laboratory animals of US National Institutes of Health (NIH), and under protocols approved by Institutional Animal Care and Use Committee at University of Southern California, and Southern Medical University

Note that full information on the approval of the study protocol must also be provided in the manuscript.